The Electrochemical Peroxydisulfate-Oxalate Autocatalytic Reaction

Jordyn N. Janusz[∇,1], Joshua A. Beeler[∇,1], Seyyedamirhossein Hosseini[1], Mayank Tanwar[2], Rui Zeng[3], Hongsen Wang[3], Héctor D. Abruña[3*], Matthew Neurock[2*], and Henry S. White[1*]

Affiliations

[1] Department of Chemistry, University of Utah, Salt Lake City, Utah 84112, United States

[2] Department of Chemical Engineering and Materials Science and Department of Chemistry, University of Minnesota, Minneapolis, Minnesota 55455, United States

[3] Department of Chemistry and Chemical Biology, Cornell University, Ithaca, New York 14853, United States

*Corresponding authors: white@chem.utah.edu; mneurock@umn.edu; hda1@cornell.edu.

ABSTRACT

Aqueous solutions containing both the strong oxidant, peroxydisulfate ($S_2O_8^{2-}$), and the strong reductant, oxalate ($C_2O_4^{2-}$), are thermodynamically unstable due to the highly exothermic homogeneous redox reaction: $S_2O_8^{2-} + C_2O_4^{2-} \rightarrow 2\ SO_4^{2-} + 2\ CO_2$ ($\Delta G^0 = -490$ kJ/mol). However, at room temperature, this reaction does not occur to a significant extent over the timescale of a day due to its inherently slow kinetics. We demonstrate that the $S_2O_8^{2-}/C_2O_4^{2-}$ redox reaction occurs rapidly, once initiated by the $Ru(NH_3)_6^{2+}$-mediated $1e^-$ reduction of $S_2O_8^{2-}$ to form $S_2O_8^{3\bullet-}$ at a glassy carbon electrode. Theoretically, the mediated electrochemical generation of a single molecule of $S_2O_8^{3\bullet-}$ is capable of initiating an *autocatalytic* cycle that consumes both $S_2O_8^{2-}$ and $C_2O_4^{2-}$ in bulk solution. Several experimental demonstrations of $S_2O_8^{2-}/C_2O_4^{2-}$ autocatalysis are presented. Differential electrochemical mass spectrometry measurements demonstrate that CO_2 is generated in solution for at least 10 minutes following a 30-s initiation step during which $S_2O_8^{3\bullet-}$

is generated. Quantitative bulk electrolysis of $S_2O_8^{2-}$ in solutions containing excess $C_2O_4^{2-}$ is initiated by electrogeneration of immeasurably small quantities of $S_2O_8^{3\bullet-}$. Capture of CO_2 as $BaCO_3$ during electrolysis additionally confirms the autocatalytic generation of CO_2. First-principles density functional theory calculations, *ab initio* molecular dynamics simulations, and finite difference simulations of cyclic voltammetric responses are presented that support and provide additional insights into the initiation and mechanism of the $S_2O_8^{2-}/C_2O_4^{2-}$ autocatalytic reaction. Preliminary evidence indicates that autocatalysis also results in a chemical traveling reaction front that propagates into the solution normal to the planar electrode surface.

Keywords: Autocatalytic reaction, electrocatalysis, peroxydisulfate, oxalate, reductive oxidation, differential electrochemical mass spectrometry.

TOC:

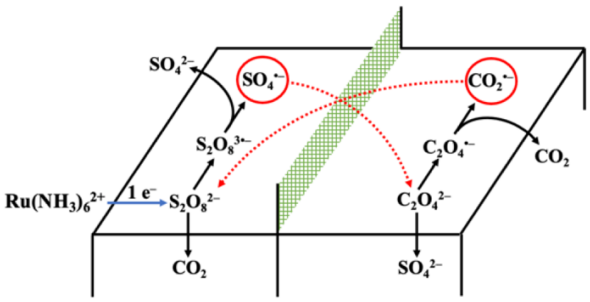

Introduction

Herein, we report on the electrochemically-initiated autocatalytic reaction between peroxydisulfate ($S_2O_8^{2-}$) and oxalate ($C_2O_4^{2-}$). $S_2O_8^{2-}$ is a strong oxidant while $C_2O_4^{2-}$ is a strong reductant, and when mixed together in aqueous solution should spontaneously react ($\Delta G^0 = -490$ kJ/mol) to yield SO_4^{2-} and CO_2, eq 1. However, since Kempf's initial observations in 1905 of

$$S_2O_8^{2-} + C_2O_4^{2-} \rightarrow 2\ SO_4^{2-} + 2\ CO_2 \qquad \Delta G^0 = -490\ \text{kJ/mol} \qquad (1)$$

aqueous solutions containing $S_2O_8^{2-}$ and $C_2O_4^{2-}$, several reports have demonstrated that the reaction, despite being thermodynamically very favored, is extremely slow in the absence of a catalyst or thermal activation.[1-3] Reports of Ag^+ catalyzed reduction of $S_2O_8^{2-}$ in the presence of reducing agents (e.g., Cr^{3+}, VO^{2+}, Mn^{2+}, Ce^{3+}, hydrazine, or ammonia) indicated that a strong oxidant is formed during $S_2O_8^{2-}$ reduction.[4-9] In addition, Ag^+ catalyzed $S_2O_8^{2-}$ reduction in the presence of $C_2O_4^{2-}$ was reported to result in the complete oxidation of $C_2O_4^{2-}$ at rates 2–3 orders of magnitude higher than systems containing the previously mentioned reducing agents.[2, 3, 9] As first proposed by Allen, these findings suggest that Ag^+ catalyzed $S_2O_8^{2-}$ reduction in the presence of $C_2O_4^{2-}$ initiates an autocatalytic reaction generating the strong transient oxidant, $SO_4^{\bullet-}$ ($E^0(SO_4^{\bullet-}/SO_4^{2-}) = 2.24$ V vs Ag/AgCl), which is capable of oxidizing $C_2O_4^{2-}$ (eq 2) to produce $CO_2^{\bullet-}$ ($E^0(CO_2^{\bullet-}/CO_2) = -2.17$ V vs Ag/AgCl), a strong reductant capable of reducing $S_2O_8^{2-}$ (eq 3).[3, 10-13]

$$C_2O_4^{2-} + SO_4^{\bullet-} \rightarrow CO_2^{\bullet-} + CO_2 + SO_4^{2-} \qquad \Delta G^0 = -170\ \text{kJ/mol} \qquad (2)$$

$$S_2O_8^{2-} + CO_2^{\bullet-} \rightarrow SO_4^{\bullet-} + SO_4^{2-} + CO_2 \qquad \Delta G^0 = -320\ \text{kJ/mol} \qquad (3)$$

The large negative free energies associated with eqs 2 and 3 suggest that, once either $SO_4^{\bullet-}$ or $CO_2^{\bullet-}$ is generated in solution, the reaction between $S_2O_8^{2-}$ and $C_2O_4^{2-}$ (eq 1) should become self-sustaining, as shown by the red arrows connecting eqs 2 and 3.

The previously reported observations that eq 1 requires initiation by a catalyst or thermal activation is understood by considering the kinetics and thermodynamics of three possible mechanisms for initiating the autocatalytic cycle, as depicted in Scheme 1. The rate constant for

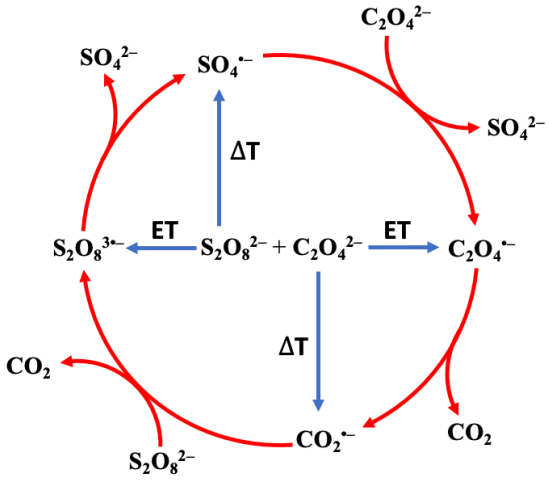

Scheme 1. Diagram showing the $S_2O_8^{2-}/C_2O_4^{2-}$ reaction where the autocatalytic cycle (red arrows) can be initiated by any one of three possible mechanisms (blue arrows): (1) thermal activation of $S_2O_8^{2-}$ to generate $SO_4^{\bullet-}$, (2) thermal activation of $C_2O_4^{2-}$ to generate $CO_2^{\bullet-}$, or (3) the 1-electron transfer (ET) from $C_2O_4^{2-}$ to $S_2O_8^{2-}$ to generate $S_3O_8^{3\bullet-}$ and $C_2O_4^{\bullet-}$, which rapidly dissociate to form $SO_4^{\bullet-}$ and $CO_2^{\bullet-}$. As discussed in the text, none of these reactions occur at a sufficient rate at room-temperature to initiate the autocatalytic reaction.

$S_2O_8^{2-}$ bond homolysis at room temperature, eq 4, is estimated to be on the order of 10^{-8} s^{-1} with an activation energy barrier of ~140 kJ/mol.[14, 15] Similarly, the activation energy barrier for

$$S_2O_8^{2-} \rightleftarrows 2\ SO_4^{\bullet-} \qquad k_f^4 \approx 10^{-8}\ s^{-1} \qquad (4)$$

$C_2O_4^{2-}$ bond homolysis, eq 5, is reported to be ~200 kJ/mol, such that, at room temperature, $k_f^5 \approx 10^{-17}\ s^{-1}$.[16]

$$C_2O_4^{2-} \rightleftarrows 2\ CO_2^{\bullet-} \qquad k_f^5 \approx 10^{-17}\ s^{-1} \qquad (5)$$

Initiation of eq 1 via eqs 4 or 5 can therefore be ruled out on kinetic grounds. (Details of how k_f^4 and k_f^5 were estimated are presented in the Supporting Information.)

Initiation of autocatalysis is also possible via the one-electron transfer from $C_2O_4^{2-}$ to $S_2O_8^{2-}$ (eq 6, labeled as ET in Scheme 1). However, this reaction has a positive free energy change of 83 kJ/mol, and is non-spontaneous based on thermodynamic considerations. To confirm that the autocatalytic reaction between $S_2O_8^{2-}$ and $C_2O_4^{2-}$ does not rapidly occur at room temperature without a catalyst, the cyclic voltammetric (CV) response of a solution containing 10 mM $S_2O_8^{2-}$ and 10 mM $C_2O_4^{2-}$ was recorded before and after allowing the solution to sit for 24 hours, Figure S1. No significant decrease in the voltammetric currents associated with $S_2O_8^{2-}$ reduction or $C_2O_4^{2-}$ oxidation was observed, demonstrating that both species are stable and that eq 6 does not occur to an appreciable extent over the course of a day.

$$S_2O_8^{2-} + C_2O_4^{2-} \rightleftarrows S_2O_8^{3\bullet-} + C_2O_4^{\bullet-} \qquad \Delta G^0 = 83\ \text{kJ/mol} \qquad (6)$$

In principle, the initiation of the $S_2O_8^{2-}/C_2O_4^{2-}$ autocatalytic reaction should be possible by either the one-electron electrochemical reduction of $S_2O_8^{2-}$ or by the one-electron oxidation of $C_2O_4^{2-}$; an idea initially proposed in 1980 by A. J. Bard to one of the authors (HSW). However, the direct reduction of $S_2O_8^{2-}$ and oxidation of $C_2O_4^{2-}$ at an electrode both occur by the rapid overall transfer of two electrons, preventing the formation in solution of either $SO_4^{\bullet-}$ or $CO_2^{\bullet-}$ necessary to initiate the autocatalytic sequence, eqs 2 and 3, *vide infra*. As such, and to the best of

our knowledge, the electrochemical initiation of the $S_2O_8^{2-}/C_2O_4^{2-}$ autocatalytic reaction has not been previously reported.

Herein, we show that very efficient electrochemical initiation of the $S_2O_8^{2-}/C_2O_4^{2-}$ autocatalytic reaction is made possible by using an outer-sphere redox electrocatalyst, $Ru(NH_3)_6^{3+/2+}$, to reduce $S_2O_8^{2-}$ in solution. We show that the $1e^-$ mediated reduction of $S_2O_8^{2-}$ by electrogenerated $Ru(NH_3)_6^{2+}$ occurs at distances sufficiently far from the electrode surface (i.e., tens of micrometers) that the direct reduction of $SO_4^{\bullet-}$ at the electrode is dramatically mitigated (and entirely eliminated under optimal conditions), thus, allowing eq 2 to proceed in initiating autocatalysis. Cyclic voltammetry is employed to investigate the mechanism and kinetics of the mediated $S_2O_8^{2-}/C_2O_4^{2-}$ autocatalytic reaction, while controlled-potential bulk electrolysis (CPE) is used to measure the amount of electrical charge required to initiate autocatalysis. Differential electrochemical mass spectrometry (DEMS) is also used to demonstrate that the $S_2O_8^{2-}/C_2O_4^{2-}$ autocatalytic reaction generates CO_2 for ~10 minutes after the reaction is initiated, without the input of additional electrical charge. The DEMS results unequivocally demonstrate that eqs 2 and 3 represent a coupled and self-sustaining reaction pair. In-depth mechanistic analysis of the $S_2O_8^{2-}/C_2O_4^{2-}$ autocatalytic reaction using first-principles density functional theory calculations (DFT), *ab initio* molecular dynamics simulations (AIMD), and finite difference (FD) simulations of the voltammetric response, support the proposed autocatalytic mechanism.

Results and Discussion

The results and discussion are presented in the following order. In Section I, we provide a brief overview of the electrochemical reduction of $S_2O_8^{2-}$ and oxidation of $C_2O_4^{2-}$. In Section II,

we demonstrate that the heterogeneous reduction of $S_2O_8^{2-}$ at a glassy carbon (GC) electrode in the presence of only $C_2O_4^{2-}$ does not lead to autocatalysis, a consequence of the direct reduction of $SO_4^{\bullet-}$ at the GC electrode. In Section III, the mediated reduction of $S_2O_8^{2-}$ using the $Ru(NH_3)_6^{3+/2+}$ couple is shown using cyclic voltammetry to initiate rapid autocatalysis in the presence of $C_2O_4^{2-}$. DEMS results monitoring CO_2 production after the initiation step is terminated are also presented in this section. In Section IV, CPE experiments are used to determine the electrical charge passed during electrolysis of bulk solutions of $S_2O_8^{2-}$ and $C_2O_4^{2-}$. Coulometric analysis of CPE experiments show that the charge necessary to initiate autocatalytic bulk electrolysis is immeasurably small. CO_2 capture during bulk CPE by the precipitation of $BaCO_3$ is also presented to demonstrate rapid CO_2 generation via the autocatalytic reaction. Finally, in Section V, a detailed autocatalytic mechanism is proposed based on DFT, AIMD, and FD simulations.

I. $S_2O_8^{2-}$ and $C_2O_4^{2-}$ Electrochemistry

Electrochemical $S_2O_8^{2-}$ reduction is well-established to proceed through an ECE mechanism (eqs 7–9).[10, 11, 17, 18] Briefly, $S_2O_8^{2-}$ is first reduced to $S_2O_8^{3\bullet-}$ (eq 7) which dissociates within ~1 ps to yield SO_4^{2-} and $SO_4^{\bullet-}$ (eq 8).[18, 19] The strongly oxidizing $SO_4^{\bullet-}$ can then be reduced to SO_4^{2-} (eq 9), resulting in the overall two-electron reduction of $S_2O_8^{2-}$ to two SO_4^{2-} (eq 10).[17-19]

Figure 1 shows the CV response of $S_2O_8^{2-}$ reduction at a GC electrode. All voltammetric data were collected using a single-compartment three-electrode cell in an O_2-free aqueous 0.1 M Na_2SO_4 solution. A notable feature of $S_2O_8^{2-}$ reduction is that its direct electrochemical reduction is observed at ~ –1.2 V vs Ag/AgCl (Figure 1, blue trace), meaning that an ~1.5 V kinetic overpotential, due to slow heterogenous electron transfer, is required to observe its direct reduction

at the GC electrode. However, the homogenous $1e^-$ reduction of $S_2O_8^{2-}$ is theoretically possible using an outer-sphere redox mediator with a standard potential (E^0) more negative than E^0 for eq 7, a strategy introduced later for initiating the autocatalytic reaction.[20]

$$S_2O_8^{2-} + e^- \rightarrow S_2O_8^{3\bullet-} \qquad E^0 = 0.33 \text{ V vs Ag/AgCl} \qquad (7)$$

$$S_2O_8^{3\bullet-} \rightarrow SO_4^{2-} + SO_4^{\bullet-} \qquad k_f^8 > 2 \text{ x } 10^{11} \text{ s}^{-1} \qquad (8)$$

$$SO_4^{\bullet-} + e^- \rightarrow SO_4^{2-} \qquad E^0 = 2.24 \text{ V vs Ag/AgCl} \qquad (9)$$

$$S_2O_8^{2-} + 2\ e^- \rightarrow 2\ SO_4^{2-} \qquad E^0_{\text{overall}} = 1.73 \text{ V vs Ag/AgCl} \qquad (10)$$

Much like $S_2O_8^{2-}$ reduction, the electrochemical oxidation of $C_2O_4^{2-}$ proceeds via an ECE mechanism that has been extensively studied.[12, 13, 21-24] In summary, the $1e^-$ oxidation of $C_2O_4^{2-}$ generates $C_2O_4^{\bullet-}$ (eq 11), which undergoes bond cleavage within ~1 μs to yield CO_2 and the strongly reducing $CO_2^{\bullet-}$ (eq 12).[12, 22] As shown in eq 13, $CO_2^{\bullet-}$ can then undergo direct oxidation at $E > -2.17$ V vs Ag/AgCl to generate a second equivalent of CO_2.[22] Notably, and in contrast to $S_2O_8^{2-}$ reduction, the direct oxidation of $C_2O_4^{2-}$ at a GC electrode occurs at potentials close to the thermodynamic value ($E^0 = 1.2$ V) associated with the first electron transfer, eq 11 (Figure 1, green trace), indicating that reaction (11) is moderately fast on voltammetric timescales.

$$C_2O_4^{2-} \rightarrow C_2O_4^{\bullet-} + e^- \qquad E^0 = 1.2 \text{ V vs Ag/AgCl} \qquad (11)$$

$$C_2O_4^{\bullet-} \rightarrow CO_2 + CO_2^{\bullet-} \qquad k_f^{12} = 5.5 \text{ x } 10^5 \text{ s}^{-1} \qquad (12)$$

$$CO_2^{\bullet-} \rightarrow CO_2 + e^- \qquad E^0 = -2.17 \text{ V vs Ag/AgCl} \qquad (13)$$

$$C_2O_4^{2-} \rightarrow 2\ CO_2 + 2\ e^- \qquad E^0_{\text{overall}} = -0.84 \text{ V vs Ag/AgCl} \qquad (14)$$

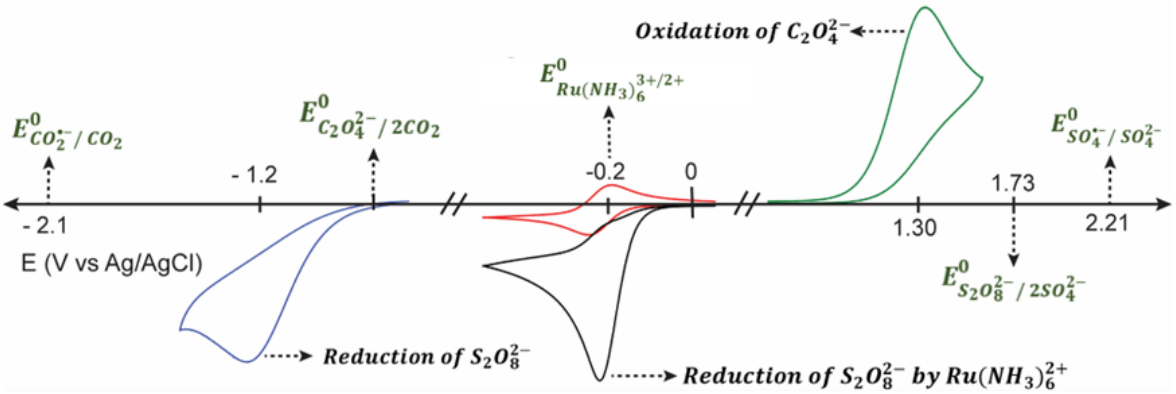

Figure 1. Voltammetric responses for the reduction of 10 mM $S_2O_8^{2-}$ (blue trace), oxidation of 10 mM $C_2O_4^{2-}$ (green trace), reduction of 0.5 mM $Ru(NH_3)_6^{3+}$ without (red trace) and with 5.0 mM $S_2O_8^{2-}$ (black trace). All voltammograms were recorded at scan rate of 100 mV/s in an O_2-free aqueous solution contaning 0.1 M Na_2SO_4 (pH = 6.8) using a 1.49-mm radius GC working electrode.

II. Direct $S_2O_8^{2-}/C_2O_4^{2-}$ Autocatalysis

Upon the reduction of $S_2O_8^{2-}$, one can envision the scenario presented in Scheme 2 where electrogenerated $SO_4^{\bullet-}$ homogeneously oxidizes $C_2O_4^{2-}$ to $C_2O_4^{\bullet-}$ (eq 15, $\Delta G^0 = -100$ kJ/mol) to liberate the strongly reducing $CO_2^{\bullet-}$ (eq 12, $\Delta G^0 = -70$ kJ/mol). $CO_2^{\bullet-}$ can subsequently reduce $S_2O_8^{2-}$ to the short lived $S_2O_8^{3\bullet-}$ in solution (eq 16, $\Delta G^0 = -240$ kJ/mol), resulting in the generation of $SO_4^{\bullet-}$ via eq 8 ($\Delta G^0 = -80$ kJ/mol). Theoretically, in the presence of $C_2O_4^{2-}$, the input of a single electron into $S_2O_8^{2-}$ (eq 7) can initiate the redox neutral $S_2O_8^{2-}/C_2O_4^{2-}$ autocatalytic reaction (Scheme 2, red arrows and eqs 8, 15, 12, and 16). Details of how ΔG^0 values were estimated from literature data can be found in the Supporting Information.

$$C_2O_4^{2-} + SO_4^{\bullet-} \rightarrow C_2O_4^{\bullet-} + SO_4^{2-} \qquad \Delta G^0 = -100 \text{ kJ/mol} \qquad (15)$$

$$S_2O_8^{2-} + CO_2^{\bullet-} \rightarrow S_2O_8^{3\bullet-} + CO_2 \qquad \Delta G^0 = -240 \text{ kJ/mol} \qquad (16)$$

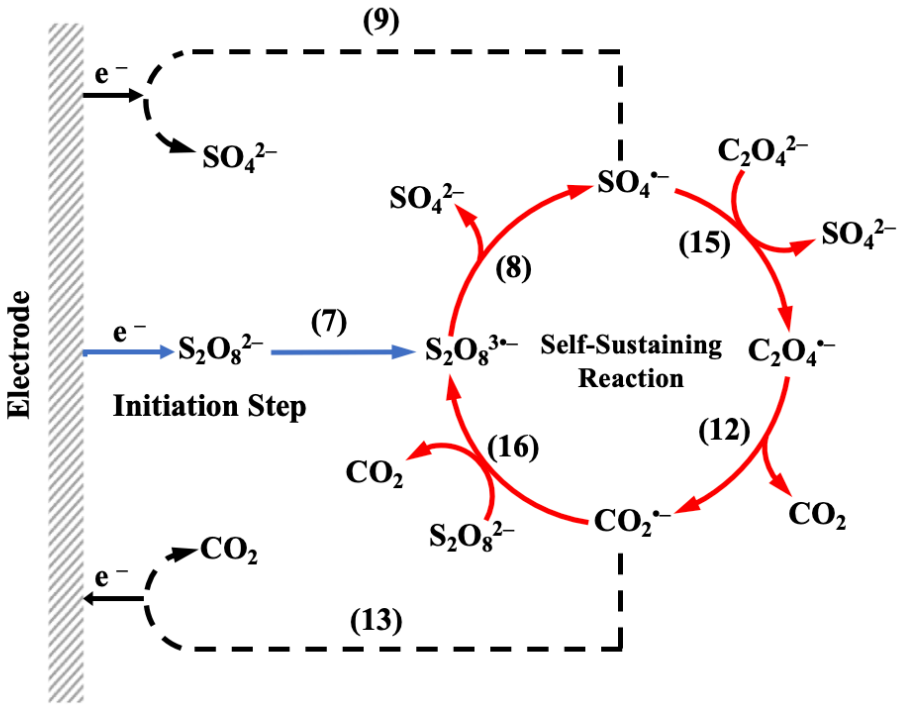

Scheme 2. Diagram depicting the direct $S_2O_8^{2-}/C_2O_4^{2-}$ autocatalytic reaction that includes an initiation step (blue arrows, direct reduction of $S_2O_8^{2-}$) and the autocatalytic reaction (red arrows) between $S_2O_8^{2-}$ and $C_2O_4^{2-}$. The dissociation of $S_2O_8^{3\bullet-}$ within ~1 nm of the electode surface results in direct reduction of $SO_4^{\bullet-}$ at the electrode (reaction (9)), preventing a self-sustaining reaction from being initiated. Reaction numbers are shown corresponding to reactions in the text.

Cyclic voltammetry was first used to determine whether direct $S_2O_8^{2-}$ reduction could initiate the $S_2O_8^{2-}/C_2O_4^{2-}$ autocatalytic reaction. Figure 2 demonstrates that the voltammetric response for the reduction of 4.0 mM $S_2O_8^{2-}$ is essentially unchanged in the presence of 4.0 mM $C_2O_4^{2-}$. If the $S_2O_8^{2-}/C_2O_4^{2-}$ autocatalytic reaction was initiated by direct reduction of $S_2O_8^{2-}$ at the electrode, additional $S_2O_8^{2-}$ would be consumed in solution according to Scheme 2, and the current associated with $S_2O_8^{2-}$ reduction at the GC electrode would decrease. As expected, the CV responses demonstrate that the $S_2O_8^{2-}/C_2O_4^{2-}$ autocatalytic reaction cannot be initiated by direct $S_2O_8^{2-}$ reduction. Additionally, CPE of $S_2O_8^{2-}$ in the presence of $C_2O_4^{2-}$ does not lead to

autocatalysis, *vide infra*. These results are consistent with the reported short lifetime of $S_2O_8^{3\bullet-}$ (~1 ps). An estimate of the distance that $S_2O_8^{3\bullet-}$ diffuses from the electrode prior to generating $SO_4^{\bullet-}$, is obtained from $\delta^2 = 2Dt$, where D is the diffusion coefficient of $S_2O_8^{3\bullet-}$ (~ 10^{-5} cm^2/s). Based on the rate of eq 8, ($k_f^8 > 2 \times 10^{11}$ s^{-1}), $t < 5 \times 10^{-12}$ s, one can demonstrate that $SO_4^{\bullet-}$ is generated within 1 nm of the GC electrode.[17, 19] Thus, the probability of $SO_4^{\bullet-}$ being further reduced at the electrode prior to encountering and oxidizing $C_2O_4^{2-}$ (eq 15) is anticipated to be essentially unity.

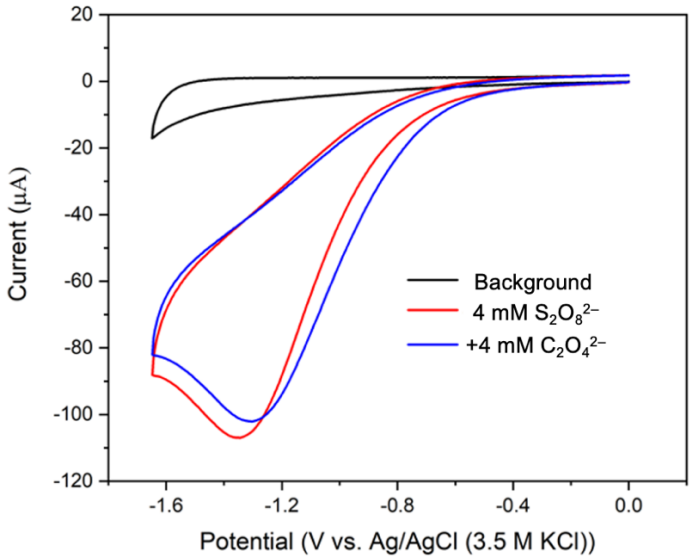

Figure 2. Cyclic voltammograms recorded in a solution containing 0.1 M Na_2SO_4 (black trace); 0.1 M Na_2SO_4 and 4.0 mM $S_2O_8^{2-}$ (red trace); and 0.1 M Na_2SO_4, 4.0 mM $S_2O_8^{2-}$, and 4.0 mM $C_2O_4^{2-}$ (blue trace). All voltammograms were recorded at a scan rate of 100 mV/s using a 1.49-mm radius GC working electrode in an O_2-free aqueous solution.

III. Mediated $S_2O_8^{2-}/C_2O_4^{2-}$ Autocatalysis

The outer-sphere redox couple $Ru(NH_3)_6^{3+/2+}$ was employed as a mediator to transfer a single electron to $S_2O_8^{2-}$, thereby mitigating $SO_4^{\bullet-}$ formation near the working electrode.[19] The reversible 1e^- reduction of $Ru(NH_3)_6^{3+}$ occurs at ~ –0.2 V vs Ag/AgCl to yield $Ru(NH_3)_6^{2+}$ (eq

17). The reversible CV response obtained in a 0.5 mM $Ru(NH_3)_6^{3+}$ solution is shown in Figure 3, black trace.[25, 26] In contrast, in the presence of 1.0 mM $S_2O_8^{2-}$, a large irreversible voltammogram is observed that is associated with the catalytically mediated reduction of $S_2O_8^{2-}$ by electrogenerated $Ru(NH_3)_6^{2+}$, resulting in regeneration of $Ru(NH_3)_6^{3+}$ and the generation of $S_2O_8^{3\bullet-}$, Figure 3, red trace. This irreversible CV response has been described in a prior report and is

$$Ru(NH_3)_6^{3+} + e^- \rightleftarrows Ru(NH_3)_6^{2+} \qquad E^0 = -0.197 \text{ V vs Ag/AgCl} \qquad (17)$$

$$Ru(NH_3)_6^{2+} + S_2O_8^{2-} \rightarrow Ru(NH_3)_6^{3+} + S_2O_8^{3\bullet-} \qquad k_f^{18} = 2.0 \times 10^5 \text{ M}^{-1}\text{s}^{-1} \qquad (18)$$

$$SO_4^{\bullet-} + Ru(NH_3)_6^{2+} \rightarrow SO_4^{2-} + Ru(NH_3)_6^{3+} \qquad k_f^{19} > 10^9 \text{ M}^{-1}\text{s}^{-1} \qquad (19)$$

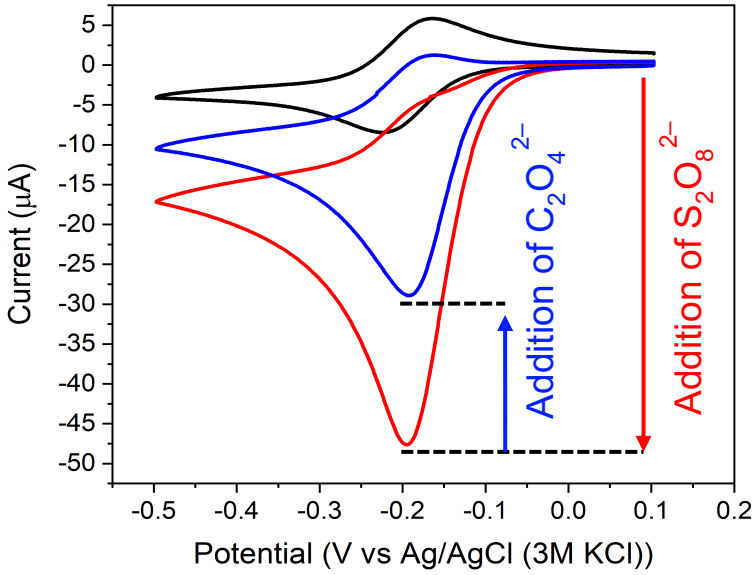

Figure 3. Cyclic voltammograms of a solution containing 0.5 mM $Ru(NH_3)_6^{3+}$ (black trace); 0.5 mM $Ru(NH_3)_6^{3+}$ and 1.0 mM $S_2O_8^{2-}$ (red trace); and 0.5 mM $Ru(NH_3)_6^{3+}$, 1.0 mM $S_2O_8^{2-}$, and 10 mM $C_2O_4^{2-}$ (blue trace). All voltammograms were recorded at 100 mV/s using a 1.49-mm radius GC working electrode in an O_2-free aqueous solution containing 0.1 M Na_2SO_4 (pH = 6.8).

ascribed to a five-step EC'CEC mechanism (eqs 17, 18, 8, 9, and 19).[19] Values of k_f[18] and k_f[19] have been previously reported and are based, respectively, on CV and scanning electrochemical microscopy analyses, while k_f[8] was estimated from DFT predictions.[19, 27] Detailed simulations of this mechanism demonstrated that electrogenerated $Ru(NH_3)_6^{2+}$ reduces $S_2O_8^{2-}$ in solution (eq 18) such that $SO_4^{\bullet-}$ is formed at distances up to ~100 μm away from the GC electrode, thereby enabling $SO_4^{\bullet-}$ to be used in an electroorganic synthetic application.[19] Based on similar reasoning, we propose that the mediated reduction of $S_2O_8^{2-}$ yields $SO_4^{\bullet-}$ sufficiently far from the electrode to be effective in oxidizing $C_2O_4^{2-}$ to initiate the $S_2O_8^{2-}/C_2O_4^{2-}$ autocatalytic reaction shown in Scheme 3.

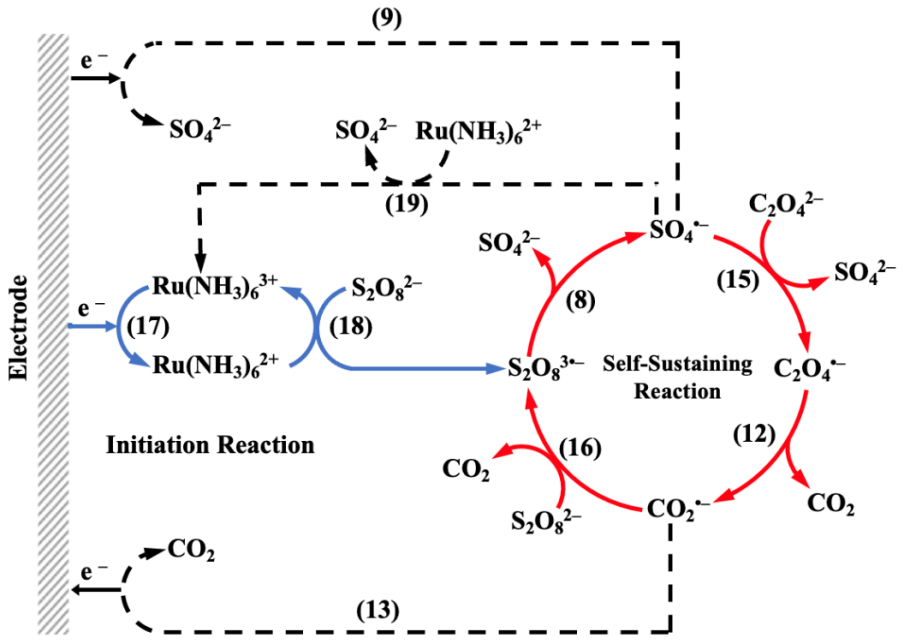

Scheme 3. Diagram depicting a plausible mechanism for the mediated $S_2O_8^{2-}/C_2O_4^{2-}$ autocatalytic reaction, which includes an initiation step (blue arrows, $Ru(NH_3)_6^{2+}$ mediated reduction of $S_2O_8^{2-}$) and the autocatalytic reaction (red arrows) between $S_2O_8^{2-}$ and $C_2O_4^{2-}$. The autocatalytic cycle can be quenched by the homogeneous oxidation of $Ru(NH_3)_6^{2+}$ by $SO_4^{\bullet-}$, or by the two electrode reactions: $CO_2^{\bullet-}$ oxidation or $SO_4^{\bullet-}$ reduction at the GC electrode (dashed lines). Reaction numbers are shown corresponding to reactions in the text.

The effect of adding 10 mM $C_2O_4^{2-}$ to the solution containing 0.5 mM $Ru(NH_3)_6^{3+}$ and 1.0 mM $S_2O_8^{2-}$ is shown in Figure 3. Upon addition of $C_2O_4^{2-}$, the CV displays both a *decrease* in the cathodic peak current and the partial *reappearance* of the anodic peak (Figure 3, blue trace). This observation suggests that once $S_2O_8^{2-}$ is reduced by $Ru(NH_3)_6^{2+}$ to form $SO_4^{\bullet-}$ (eq 18), the $S_2O_8^{2-}$ /$C_2O_4^{2-}$ autocatalytic cycle shown in Scheme 3 is initiated, resulting in $S_2O_8^{2-}$ being consumed by reaction with $CO_2^{\bullet-}$ (eq 16) rather than through the mediated reduction by $Ru(NH_3)_6^{2+}$ (eq 18). Further increases in the concentration of $C_2O_4^{2-}$ result in a continuous decrease in the cathodic peak current and increase in the anodic peak current resulting in a reversible response resembling that of a solution containing only $Ru(NH_3)_6^{3+}$ (see Figure S2). Thus, the CV results are consistent with the idea that eqs 17 and 18 initiate the $S_2O_8^{2-}$/$C_2O_4^{2-}$ autocatalytic reaction (eq 1).

Scheme 3 indicates that 2 molecules of CO_2 are generated during each cycle of the $S_2O_8^{2-}$ /$C_2O_4^{2-}$ autocatalytic reaction. To test this prediction, DEMS, a powerful *operando* method useful in real time monitoring of electrogenerated gaseous and/or volatile species, was used to detect CO_2 produced by the autocatalytic reaction.[28] Cyclic voltammetry was performed using a porous carbon cloth as the working electrode, while monitoring the mass spectrometer ion currents at m/z = 44 (ionized CO_2, CO_2^+) and 22 (doubly ionized CO_2, CO_2^{2+}). Briefly, any CO_2 generated by the autocatalytic reaction diffuses through the carbon cloth electrode, eventually partitioning out of the electrolyte phase into the DEMS sample inlet (see the SI for a more detailed description). In a set of control experiments, no signal associated with potential-induced CO_2 generation was detected during CV scans between 0.1 and –0.5 V vs Ag/AgCl in: (*i*) a 0.1 M Na_2SO_4 background solution; (*ii*) a solution containing 0.1 M Na_2SO_4 and 0.5 mM $Ru(NH_3)_6^{3+}$; or (*iii*) a solution containing 0.1 M Na_2SO_4, 0.5 mM $Ru(NH_3)_6^{3+}$ and 100 mM $C_2O_4^{2-}$ (Figure S3). However, when a voltammetric scan was performed in a solution containing 0.5 mM $Ru(NH_3)_6^{3+}$, 100 mM $C_2O_4^{2-}$

, and 1.0 mM $S_2O_8^{2-}$, ionic currents for CO_2^+ (m/z = 44) and CO_2^{2+} (m/z = 22) were observed in the DEMS response, as shown in Figure 4 and Figure S3. These observations unequivocally establish that CO_2 is generated during the $Ru(NH_3)_6^{2+}$ catalyzed reduction of $S_2O_8^{2-}$ in the presence of $C_2O_4^{2-}$.

The DEMS methodology also provides a direct demonstration of the self-sustaining nature of the autocatalytic reaction, as suggested in Scheme 3. In the experiment corresponding to Figure 4, the ionic current associated with CO_2^+ (m/z = 44) generation was monitored during and following a single CV cycle in which the electrode potential was cycled between 0.1 and –0.5 V, and then back to 0.1 V, where it was held constant. As shown in Figure 4, at a scan rate of 20 mV/s, the CO_2^+ signal initially exhibits a rapid increase on the negative scan direction upon reduction of $Ru(NH_3)_6^{3+}$ until the potential reaches –0.22 V, corresponding approximately to the peak potential for $Ru(NH_3)_6^{3+}$ reduction. The CO_2^+ signal then slowly decreases due to the consumption of $C_2O_4^{2-}$ and reduced generation of CO_2 near the carbon cloth electrode. However, as shown later in Section V, the autocatalytic reaction continues to propagate through the solution, continuing to generate CO_2 at distances further from the electrode and DEMS sample inlet. After completion of the CV scan and while the electrode potential was held at 0.1 V, CO_2^+ remained detectable for an additional ~600 s before decaying to the background level. These results demonstrate that CO_2 is continuously generated and can be detected for at least ~10 minutes following cessation of the $Ru(NH_3)_6^{2+}$-catalyzed reduction of $S_2O_8^{2-}$. Similar results were observed at both 10 mV/s and 5 mV/s, Figure 4. These results directly demonstrate that the $S_2O_8^{2-}$ /$C_2O_4^{2-}$ autocatalytic reaction is *self-sustaining*, once initiated by generation of a finite quantity of $S_2O_8^{3\bullet-}$ (eq 18), *i.e.*, the autocatalyic cycle does not require the additional external input of electrons. Additional DEMS experiments supporting CO_2 generation are presented in the SI.

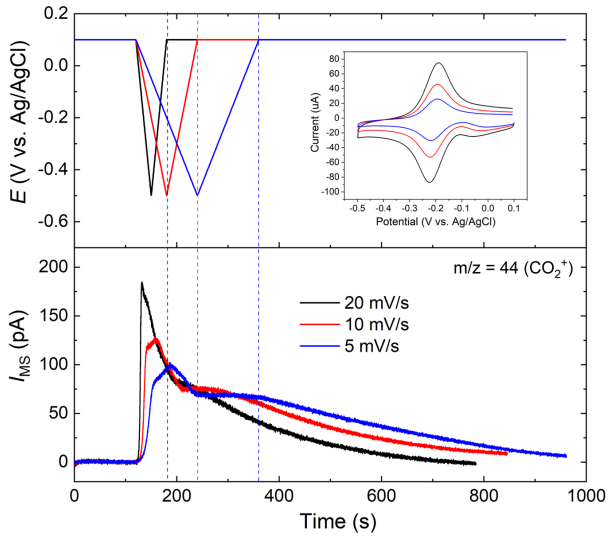

Figure 4. DEMS analysis of CO_2 formation in an aqueous solution containing 0.5 mM $Ru(NH_3)_6^{3+}$, 200 mM $C_2O_4^{2-}$, 1.0 mM $S_2O_8^{2-}$, and 0.1 M Na_2SO_4. The mass spectrometric signal for CO_2^+ (m/z = 44) was monitored for CVs carried out at scan rates of 5 (blue trace), 10 (red trace), and 20 mV/s (black trace). The top panel shows the applied *E*-*t* waveforms, and the inset displays the corresponding CVs. The bottom panel shows the mass spectrometric signal vs time. The dashed vertical lines indicate the end of the voltammetric cycle where the electrode potential was held constant at 0.1 V vs Ag/AgCl.

IV. Controlled-Potential Electrolysis

CPE experiments were performed in a three-electrode, divided cell using a reticulated vitreous carbon (RVC) working electrode (~175 cm^2) in the cathodic compartment, held at –0.35 V vs Ag/AgCl (*i.e.*, at a potential corresponding to diffusion-limited $Ru(NH_3)_6^{3+}$ reduction). The Ag/AgCl reference electrode was placed in the cathode compartment, which contained 24 mL of solution. The anode compartment contained a graphite rod counter electrode (~50 cm^2) immersed in 20 mL of a 0.1 M Na_2SO_4 solution (pH = 6.8), separated from the cathode compartment by a porous glass frit and a permeable ion exchange membrane made of 3 M KCl solution in agar. A

detailed description of the cell and electrolysis procedure is discussed in the Supporting Information.

Figure 5 shows typical electrolysis *i-t* curves corresponding to: (A) a solution containing $Ru(NH_3)_6^{3+}$ and $S_2O_8^{2-}$ and (B) a solution containing $Ru(NH_3)_6^{3+}$, $S_2O_8^{2-}$, and $C_2O_4^{2-}$. In both cases, the *i-t* curve displays an exponential decay, with the current decreasing to zero when $Ru(NH_3)_6^{3+}$ and $S_2O_8^{2-}$ are both fully reduced. Note that $Ru(NH_3)_6^{3+}$ is reduced to $Ru(NH_3)_6^{2+}$ once $S_2O_8^{2-}$ is fully consumed by either reaction with $Ru(NH_3)_6^{2+}$ or via the autocatalytic reaction. We also note that in the presence of $C_2O_4^{2-}$, Figure 5B, it is theoretically possible that the oxidation of $CO_2^{\bullet-}$, eq 13 and Scheme 3, may contribute to the electrolysis current, which would lower the observed cathodic current due to $Ru(NH_3)_6^{3+}$ and $S_2O_8^{2-}$ reduction. However, $CO_2^{\bullet-}$ is generated homogeneously away from the electrode surface as a transient species and is always present at very low concentrations (< 1 nM, *vide infra*, see simulated concentration profiles in Section V) and, thus, does not significantly contribute to the overall electrolysis current.

The charge passed in a CPE experiment, Q (coulombs), corresponding to the shaded areas under the *i-t* traces, is given by (eq 20), where i is the time-dependent electrolysis current.

$$Q = \int_0^t i\mathrm{d}t \qquad (20)$$

Comparison of the results shown in Figures 5A and B, demonstrates that the Q associated with the $Ru(NH_3)_6^{3+}$ mediated reduction of $S_2O_8^{2-}$ in the presence of 220 mM $C_2O_4^{2-}$ (Q = 2.32 C, Figure 5B) is substantially lower than the value when $C_2O_4^{2-}$ is absent (Q = 6.17 C, Figure 5A). This observation is consistent with, and completely analogous to, the decrease in the CV peak current

for $Ru(NH_3)_6^{3+}$ mediated reduction of $S_2O_8^{2-}$ in the presence of $C_2O_4^{2-}$ (Figures 3 and S2), further demonstrating that that $S_2O_8^{2-}$ is consumed by the autocatalytic reaction with $C_2O_4^{2-}$ (Scheme 3).

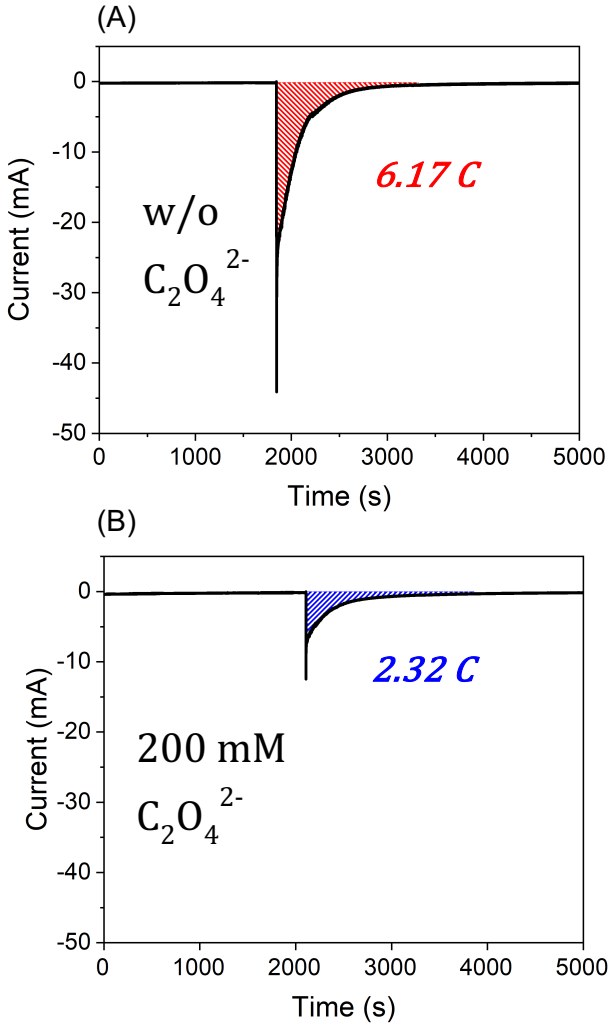

Figure 5. *i-t* traces for the CPE of 0.5 mM $Ru(NH_3)_6^{3+}$ and 1.0 mM $S_2O_8^{2-}$ (A) without $C_2O_4^{2-}$ and (B) with 200 mM $C_2O_4^{2-}$. Q = 6.17 C for the mediated reduction of $S_2O_8^{2-}$ in the absence of $C_2O_4^{2-}$ and 2.32 C for the mediated reduction of $S_2O_8^{2-}$ in the presence of 200 mM $C_2O_4^{2-}$. Both electrolyses were carried out at –0.35 V vs Ag/AgCl in a three-electrode divided cell, in an O_2-free aqueous solution containing 0.1 M Na_2SO_4 (pH = 6.50) using a RVC cathode and a graphite rod anode.

The Q measured from CPE (eq 20) can be expressed by eq 21, where n_s and n_R are the number of electrons required to reduce one molecule of $S_2O_8^{2-}$ and $Ru(NH_3)_6^{3+}$, respectively, and N_s and N_R are the number of moles of $S_2O_8^{2-}$ and $Ru(NH_3)_6^{3+}$ initially present in solution, respectively, and F is Faraday's constant. Rearrangement of eq 21 to eq 22 allows n_s to be determined from the measurement of Q and a knowledge of n_R (= 1, eq 17).

The number of autocatalytic cycles (i.e., the cyclic mechanism indicated by the red arrows in Scheme 3) resulting per electron needed to electrogenerate $S_2O_8^{3\bullet-}$ was determined by analysis of a set of CPE experiments using eq 22 to determine n_s as a function of solution composition. A value of $n_s \sim 2$ corresponds to no autocatalysis, while a value $n_s \sim 0$ indicates that the autocatalytic cycle is self-sustaining upon generation of just a few $S_2O_8^{3\bullet-}$ molecules. In an initial experiment, n_R was measured to be 0.98 by CPE at –0.35 V vs Ag/AgCl in a solution containing only $Ru(NH_3)_6^{3+}$, as expected for a $1e^-$ reduction. As noted above, CPE of a solution containing $Ru(NH_3)_6^{3+}$ and $S_2O_8^{2-}$ in the absence of $C_2O_4^{2-}$ (Figure 5A, $Q = 6.17$ C) yielded $n_s = 1.94 \pm 0.03$, as expected for the overall $2e^-$ reduction of $S_2O_8^{2-}$, eq 10. When the experiment was repeated in the presence of 200 mM $C_2O_4^{2-}$ (Figure 5A, $Q = 2.32$ C) n_s decreased significantly to a value of 0.42 ± 0.01, indicating that some fraction of $S_2O_8^{2-}$ is being consumed by the autocatalytic reaction, thereby reducing the electrical charge required to reduce all $S_2O_8^{2-}$ in solution.

$$Q_{total} = F\,(n_R N_R + n_s N_s) \qquad (21)$$

$$n_s = ((Q_{total}/F) - (n_R N_R))/N_s \qquad (22)$$

Values of n_s were then measured over a range of $C_2O_4^{2-}$, $S_2O_8^{2-}$, and $Ru(NH_3)_6^{3+}$ concentrations, with the results presented in Figure 6. With the concentrations of $Ru(NH_3)_6^{3+}$ and $S_2O_8^{2-}$ held constant at 0.5 and 1.0 mM, respectively, a decrease in n_s from 1.94 ± 0.03 to $0.34 \pm$

0.01 (Figures 6 and S11) was observed as the concentration of $C_2O_4^{2-}$ increased from 0 to 220 mM. Then, with the concentrations of $C_2O_4^{2-}$ and $S_2O_8^{2-}$ held constant at 200 and 1.0 mM, respectively, an increase in the concentration of $Ru(NH_3)_6^{3+}$ from 0.25 to 5.0 mM (Figures 6 and S12) resulted in a decrease in n_s from 0.45 ± 0.04 to 0.10 ± 0.04. Finally, at constant values of 3.5 mM $Ru(NH_3)_6^{3+}$ and 200 mM $C_2O_4^{2-}$, decreasing the concentration of $S_2O_8^{2-}$ from 10 mM to 0.5 mM resulted in a further decrease in n_s from 0.36 ± 0.05 to 0.02 ± 0.09 (Figures 6 and S13). Thus, within the experimental error of the CPE measurements, these data indicate that the solution conditions can be optimized such that a self-sustaining $S_2O_8^{2-}/C_2O_4^{2-}$ autocatalytic reaction can be initiated by injection of an vanishingly small number of electrons (*i.e.*, $n_s \sim 0$ within error of the CPE measurement).

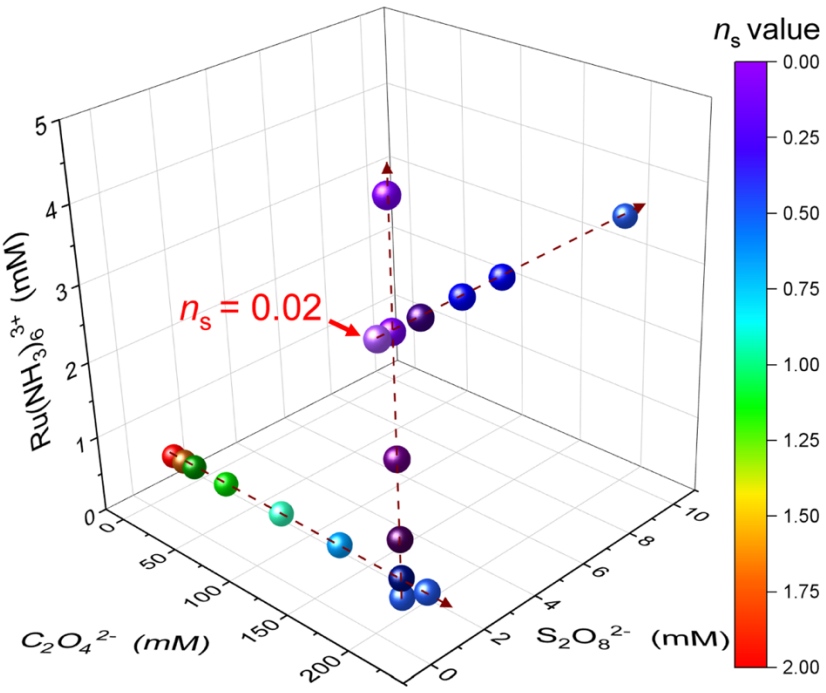

Figure 6. Plot of n_s as a function of the concentrations of $C_2O_4^{2-}$, $Ru(NH_3)_6^{3+}$, and $S_2O_8^{2-}$ in an O_2-free aqueous solution containing 0.1 M Na_2SO_4 (pH = 6.50). Electrolyses were carried out in a divided cell at –0.35 V vs Ag/AgCl.

Further evidence for the electrochemically initiated $S_2O_8^{2-}/C_2O_4^{2-}$ autocatalytic reaction was obtained by quantifying the amount of CO_2 generated through the course of CPE. CO_2 was captured during electrolysis as $BaCO_3$ by continuously flowing the gas in the headspace above the 24 mL cathodic compartment of the CPE cell through a $Ba(OH)_2$ solution. Details of the CO_2 collection experiments are presented in the Supporting Information. Electrolysis of 3.5 mM $Ru(NH_3)_6^{3+}$ at –0.35 V in the presence of 50 mM $S_2O_8^{2-}$ (1.2 mmol) and 200 mM $C_2O_4^{2-}$ resulted in n_s = 0.29 along with the recovery of 0.54 g of $BaCO_3$, corresponding to the formation of 2.7 mmol of CO_2 . Based on the volume of the electrolysis solution (24 mL) and noting that the reduction of 1 mole of $S_2O_8^{2-}$ yields 2 moles of CO_2, the electrolysis is expected to yield 2.4 mmol of CO_2, slightly less than experimentally observed. In a control experiment, 0.024 g of $BaCO_3$ were recovered during electrolysis of a solution containing only 3.5 mM $Ru(NH_3)_6^{3+}$ and 50 mM $S_2O_8^{2-}$ (no $C_2O_4^{2-}$), resulting from capture of CO_2 from the lab atmosphere. Thus, the slight excess of $BaCO_3$ recovered from the autocatalytic reaction (2.7 mmol vs 2.4 expected) most likely arises from the contribution of atmospheric CO_2. Overall, these results, consistent with the DEMS results, unambiguously demonstrate oxidation of $C_2O_4^{2-}$ by autocatalysis, Scheme 3.

The potential applied in the CPE experiments, –0.35 V, is ~1.5 V more negative than the potential at which $C_2O_4^{2-}$ is electrochemically oxidized to CO_2, *i.e.*, E^0 = 1.2 V vs Ag/AgCl, eq 11 and Figure 1. Thus, $C_2O_4^{2-}$ oxidation leading to CO_2 generation at the CPE working electrode is not feasible. The use of a divided electrolysis cell also eliminates $C_2O_4^{2-}$ oxidation at the counter electrode during electrolysis. Thus, CO_2 generation can only occur via the autocatalyic reaction.

V. Mechanistic Analysis

First-principles DFT calculations and AIMD simulations were carried out to provide a detailed atomistic understanding of the underlying reactions and energetics. In line with our previous work, we carried out periodic AIMD simulations in the canonical (NVT) ensemble using the Vienna Ab initio Simulation Package (VASP) to obtain the hydration shells for the key solution-phase species and the dynamics of radical intermediates in the solution.[29] The solvated molecular structures established from the AIMD simulations were subsequently optimized with the Gaussian-16 software program to determine the energetics for these species and the reaction energies for corresponding redox reactions (see SI for details).[30] Thermodynamic redox potentials and the inner- and outer-sphere reorganization energies were subsequently calculated and used along with Marcus theory to determine the electron-transfer barriers for reactions involved in the $S_2O_8^{2-}/C_2O_4^{2-}$ autocatalytic reaction cycle.[19, 31, 32]

Our previous work described, in detail, the mediated reduction of $S_2O_8^{2-}$ to $SO_4^{\bullet-}$ using the outer-sphere $Ru(NH_3)_6^{3+/2+}$ redox electrocatalyst.[19] $Ru(NH_3)_6^{3+}$ is first reduced at the electrode to form $Ru(NH_3)_6^{2+}$ (eq 17), which subsequently reduces $S_2O_8^{2-}$ to $S_2O_8^{3\bullet-}$ in a rate-limiting step with a free energy barrier of $\Delta G^{\ddagger} = 62$ kJ/mol and regenerates $Ru(NH_3)_6^{3+}$, eq 18 (Scheme 4). $S_2O_8^{3\bullet-}$ rapidly disproportionates to form SO_4^{2-} and the highly oxidizing $SO_4^{\bullet-}$ species (eq 8).

$C_2O_4^{2-}$ is subsequently oxidized by the highly oxidizing $SO_4^{\bullet-}$ thus generating $C_2O_4^{\bullet-}$ and SO_4^{2-} (eq 15). The one-electron oxidation potential of $C_2O_4^{2-}$ is calculated to be 0.13 V vs Ag/AgCl using an implicit water SMD solvation model, which is significantly lower than the experimental value of 1.2 V vs Ag/AgCl (eq 11). This significant difference can be attributed to the insufficient stabilization of the anionic $C_2O_4^{2-}$ and $C_2O_4^{\bullet-}$ species using implicit solvation, in line with observations in our previous work for modeling highly anionic aqueous species in the reduction of $S_2O_8^{2-}$ to $S_2O_8^{3-\bullet}$. A detailed analysis showing the variation of the oxidation potentials with DFT

methods, including the effect of the functionals and basis sets, is presented in the SI, and illustrates the critical role of solvation for these anionic species, irrespective of the methods.

The strong interactions between the anions and water are insufficiently modeled by implicit solvation continuum models. Explicitly solvated structures obtained with AIMD and optimized with DFT are used instead to bypass the limitations of the implicit solvation model where the anionic species are specifically stabilized via hydrogen bonds in the aqueous medium. The anions are stabilized by the protons acting as a Brønsted acid. These solvated structures yield an oxidation potential of 0.8 V vs Ag/AgCl, which is in better agreement with the experimental potential of 1.2 V vs Ag/AgCl (Figure 7). The hydrogen bonding with explicit solvation preferentially stabilizes the more anionic reactant $C_2O_4^{2-}$ compared to the less anionic product $C_2O_4^{\bullet-}$, thus increasing the magnitude of the electron removal energy, pushing the potential to a more positive value. With these improved energetics, Marcus theory gives a shallow free energy barrier of $\Delta G^{\ddagger} = 4\ kJ/\text{mol}$ for the oxidation of the solvated $C_2O_4^{2-}$ species by the highly oxidizing $SO_4^{\bullet-}$.

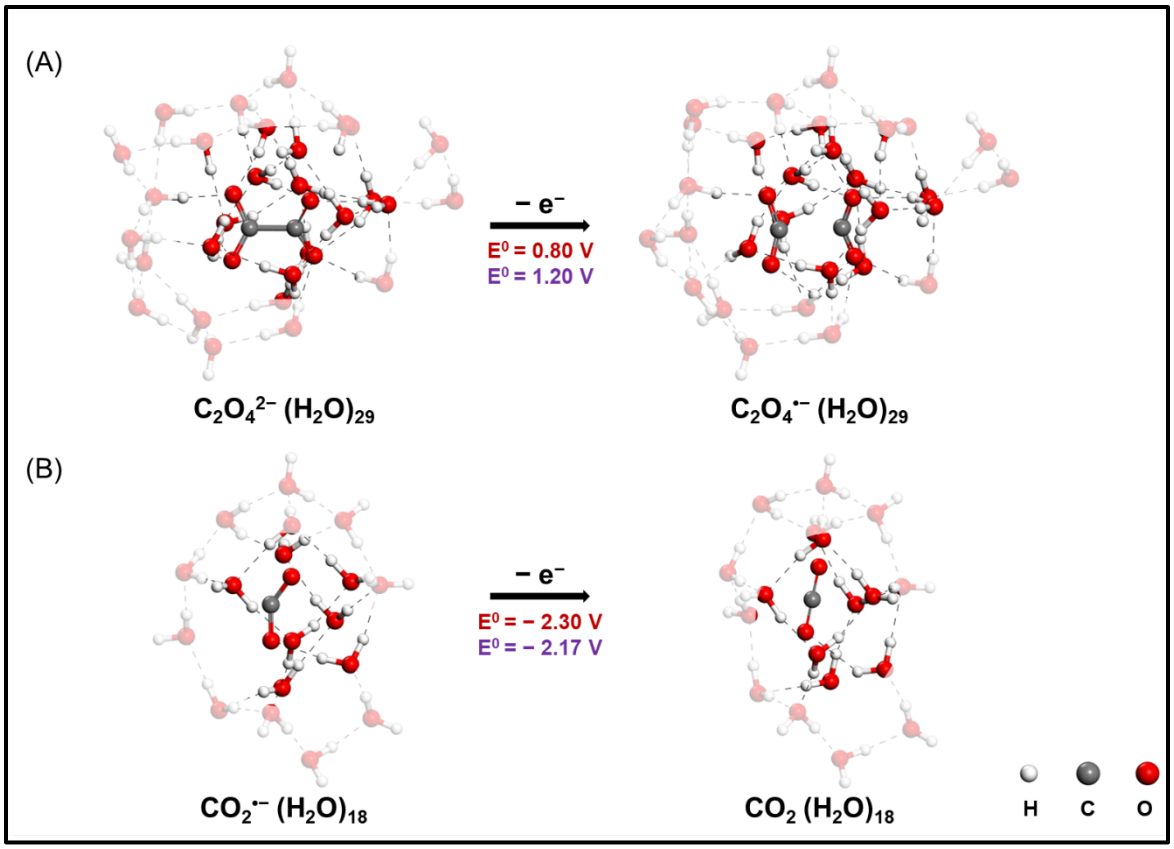

Figure 7. DFT-optimized explicit water structures for (A) $C_2O_4^{2-}$/ $C_2O_4^{\bullet-}$ (eq 11) and (B) $CO_2^{\bullet-}$/ CO_2 (eq 13) redox pairs. The E^0 values calculated from DFT are shown in red, while experimental values are in purple. All potentials are reported versus the Ag/AgCl (3.5 M KCl) reference electrode.

Upon oxidation, the C-C bond in $C_2O_4^{\bullet-}$ undergoes an elongation of about 0.25–0.30 Å (Figure 7A). Periodic AIMD simulations show similar changes in the bond length upon oxidation, with an average bond elongation of 0.33 Å (see SI for details). This is significantly shorter than the 1 Å increase in the O-O bond that occurs upon reduction of $S_2O_8^{2-}$ to $S_2O_8^{3-\bullet}$ that we reported previously.[19] The inner-sphere reorganization energy (λ_i) for $C_2O_4^{2-}$ oxidation at λ_i = 81 kJ/mol is significantly lower than the reorganization energy for $S_2O_8^{2-}$ reduction at $\lambda_i = 416$ kJ/mol, in agreement with the degree of the respective bond elongations. The lower extent of bond

elongation, together with the generation of a Lewis acid-base pair (CO_2 and $CO_2^{\bullet-}$) in $C_2O_4^{\bullet-}$ (Figure 7A), can lead to a significantly longer lifetime of $C_2O_4^{\bullet-}$ as compared to $S_2O_8^{3-\bullet}$, where no such Lewis acid-base pair is obtained ($SO_4^{\bullet-}$ and SO_4^{2-}). This observation is consistent with the numerical simulations presented later and is further supported by the results for the AIMD simulations of these four solvated species ($S_2O_8^{2-}$, $S_2O_8^{3-\bullet}$, $C_2O_4^{2-}$, and $C_2O_4^{\bullet-}$) in the aqueous phase (Figure S14), which show that $C_2O_4^{\bullet-}$ is more stable than $S_2O_8^{3-\bullet}$ over the period of our simulations.

Upon oxidation of $C_2O_4^{2-}$, $C_2O_4^{\bullet-}$ disproportionates in an ergo neutral reaction with reaction free energy of $\Delta G_{\text{reac}} = -4$ kJ/mol, eq 12, to form CO_2 and $CO_2^{\bullet-}$. The standard one-electron reduction potential of CO_2 to $CO_2^{\bullet-}$ is then computed to be –2.26 V (without) and –2.30 (with) explicit solvation. Since $CO_2^{\bullet-}$ is not highly anionic, implicit water sufficiently stabilizes this intermediate. As a result, these potentials agree reasonably well with the experimental potential of –2.17 V (eq 13). $CO_2^{\bullet-}$ is a bent species with an O-C-O angle of 134° with explicit solvation, which upon oxidation to CO_2 becomes linear (Figure 7B). This change in bond angle results in a moderately high inner-sphere reorganization energy of λ_i = 187 kJ/mol.

Being a potent reducing intermediate, $CO_2^{\bullet-}$ can reduce $Ru(NH_3)_6^{3+}$ (eq 24), which when followed by eq 18 (*i.e.*, the reduction of $S_2O_8^{2-}$ by $Ru(NH_3)_6^{2+}$) represents a pathway that is

$$CO_2^{\bullet-} + Ru(NH_3)_6^{3+} \rightarrow CO_2 + Ru(NH_3)_6^{2+} \qquad (24)$$

equivalent to the direct reduction of $S_2O_8^{2-}$ by $CO_2^{\bullet-}$ (eq 16). In other words, eqs 24 and 18 represent the $Ru(NH_3)_6^{3+/2+}$ mediated reduction of $S_2O_8^{2-}$ by $CO_2^{\bullet-}$ while eq 16 represents the

direct reduction of $S_2O_8^{2-}$ by $CO_2^{\bullet-}$. Which of these two pathways is dominant in the autocatalytic reaction is likely determined by the rate of eq 16 relative to the rates of eqs 24 and/or 18.

Figure 1 shows that the electrochemical reduction of $Ru(NH_3)_6^{3+}$ is reversible, occurring near E^0 for the $Ru(NH_3)_6^{3+/2+}$ couple, while the electrochemical reduction of $S_2O_8^{2-}$ is kinetically sluggish and requires a large overpotential.[19] In line with the kinetics of these electrode reactions, calculations from Marcus theory show that when $CO_2^{\bullet-}$ is employed as the electron source, $Ru(NH_3)_6^{3+}$ reduction occurs with a low free energy barrier of $\Delta G^{\ddagger} = 5\ kJ/\text{mol}$ as compared to $S_2O_8^{2-}$ reduction, which has a free energy barrier of $\Delta G^{\ddagger} = 43\ kJ/\text{mol}$. The low energy barrier for eq 24 suggests that $Ru(NH_3)_6^{3+}$ reduction by $CO_2^{\bullet-}$ should be a relatively fast reaction, a result used below in the simulations of the cyclic voltammetric behavior. The higher barrier for $CO_2^{\bullet-}$ reduction of $S_2O_8^{2-}$, eq 16, can be attributed to the high inner-sphere reorganization energy of $\lambda_i = 416$ kJ/mol associated with the reduction of $S_2O_8^{2-}$ to $S_2O_8^{3-\bullet}$, as there are appreciable structural changes that result from the elongation and dissociation of the peroxo bond.

The preceding DFT analysis above provides three critical results: (1) the rate-determining step (rds) in the $S_2O_8^{2-}/C_2O_4^{2-}$ autocatalytic reaction is the initial homogeneous reduction of $S_2O_8^{2-}$ by $Ru(NH_3)_6^{2+}$ (eq 18, $\Delta G^{\ddagger} = 62\ kJ/\text{mol}$); (2) the activation barrier for the reduction of $Ru(NH_3)_6^{3+}$ by $CO_2^{\bullet-}$ (eq 24, $\Delta G^{\ddagger} = 5\ kJ/\text{mol}$) is lower than the barrier for the reduction of $S_2O_8^{2-}$ by $CO_2^{\bullet-}$ (eq 16, $\Delta G^{\ddagger} = 43\ kJ/\text{mol}$); (3) the overall activation energy barriers for eqs 18 and 24 are greater than that for eq 16. Scheme 4 shows the overall proposed autocatalytic mechanism, with the inclusion of the possibility of eqs 24 and 18 (path B) occurring in parallel to eq 16 (path A). Activations energies determined by DFT are shown adjacent to each equation number.

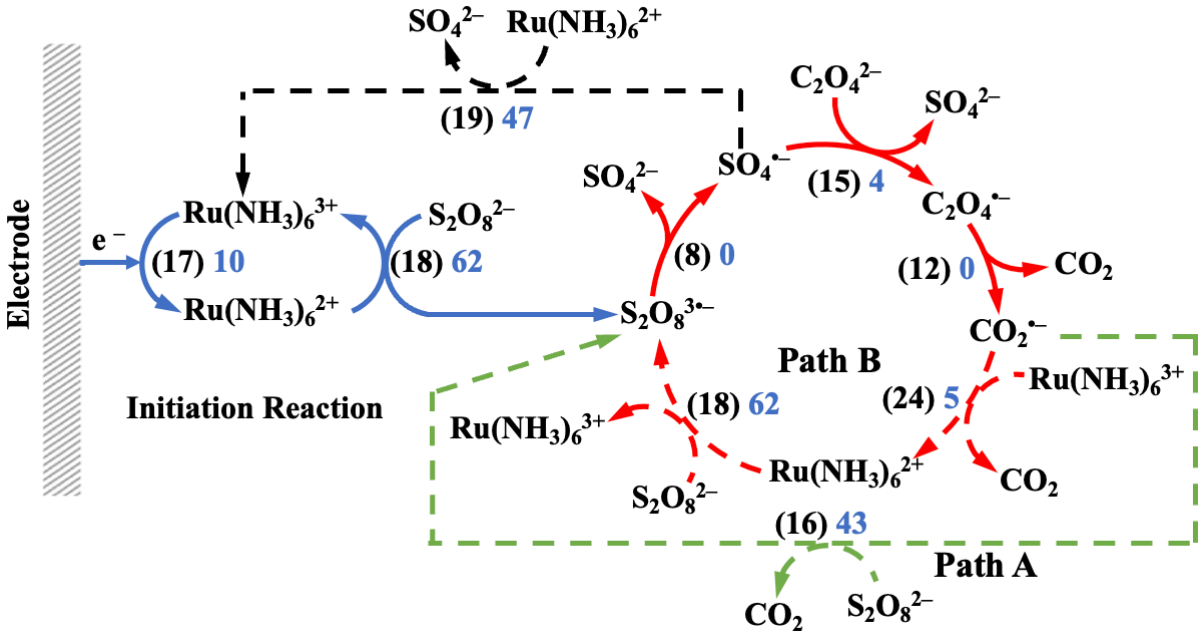

Scheme 4. The $S_2O_8^{2-}/C_2O_4^{2-}$ autocatalytic reaction initiated by redox mediated $S_2O_8^{2-}$ reduction (eq 18). Following the initiation step, the autocatalytic cycle is self-sustaining in solution (*i.e.*, an additional initiation step is not required) by eqs 8, 15, 12, 24, 18, and 16 until the limiting reactant ($S_2O_8^{2-}$) is fully consumed. DFT-calculated free energy barriers (in kJ/mol) for the proposed elementary steps are given in blue while numbers in black correspond to the equation numbers given in the text. The zero free energy barriers correspond to intramolecular bond cleavage of $S_2O_8^{3\bullet-}$ and $C_2O_4^{\bullet-}$. Path A (green dashed line) and Path B (red dashed lines) represent the direct and indirect (*i.e.*, $Ru(NH_3)_6^{3+/2+}$ mediated) reduction of $S_2O_8^{2-}$ by $CO_2^{\bullet-}$. Wow!!!!

Guided by the DFT analysis, finite different (FD) simulations of the expected voltammetric behavior based on Scheme 4 were compared to experimental CV data to determine whether the $S_2O_8^{2-}/C_2O_4^{2-}$ autocatalytic reaction proceeds via eq 16 (Path A), or by eqs 24 and 18 (Path B), or by both pathways. As shown below, the FD simulations also provide valuable insights in the distributions and concentrations of transient $CO_2^{\bullet-}$ and $SO_4^{\bullet-}$ and suggest that the autocatalytic path should result in a chemical wave propagating away from the electrode surface.

A summary of the thermodynamic and kinetic values of the reactions used in FD simulations are given in Table 1. K_{eq} values are based on E^0 values and literature free energy data as described in the Supporting Information. With the exception of reaction 24, all rate constants listed in Table 1 are obtained from prior measurements reported in the literature. The rate constant for the reduction of $S_2O_8^{2-}$ by $Ru(NH_3)_6^{2+}$, k_f[18], was determined by cyclic voltammetry, and recently confirmed by steady-state microelectrode voltammetry and SECM.[19, 27] The rate of dissociation of $S_2O_8^{3\bullet-}$, k_f[8], was previously estimated from DFT to be > 5 x 10^{12} s^{-1}; however, the results of the FD simulations were found to be insensitive to values of k_f[8] greater than 1 x 10^6 s^{-1}.[19] Values of k_f[19] and k_f[12] were independently obtained by separate specialized SECM measurements.[22, 27] Values of k_f[15] and k_f[16] where determined by flash photolysis experiments.[33, 34] With these literature values in hand, the rate constant for reaction 24 was determined by optimizing the fit of FD simulations to the experimental CV results, as described below.

Table 1. Kinetic and thermodynamic parameters for the $S_2O_8^{2-}/C_2O_4^{2-}$ autocatalytic reaction			
Eq No.	Reaction	K_{eq} [a]	k_f [b]
18	$Ru(NH_3)_6^{2+} + S_2O_8^{2-} \rightleftarrows Ru(NH_3)_6^{3+} + S_2O_8^{3\bullet-}$	8.1 x 10^8	2 x 10^5 $M^{-1}s^{-1}$ (19)
8	$S_2O_8^{3\bullet-} \leftrightarrows SO_4^{2-} + SO_4^{\bullet-}$	1.5 x 10^{14}	> 1 x 10^6 s^{-1} (19)
19	$SO_4^{\bullet-} + Ru(NH_3)_6^{2+} \leftrightarrows SO_4^{2-} + Ru(NH_3)_6^{3+}$	1.5 x 10^{41}	> 1 x 10^9 $M^{-1}s^{-1}$ (27)
15	$C_2O_4^{2-} + SO_4^{\bullet-} \rightleftarrows C_2O_4^{\bullet-} + SO_4^{2-}$	3.9 x 10^{17}	2.1 x 10^7 $M^{-1}s^{-1}$ (33)
16	$CO_2^{\bullet-} + S_2O_8^{2-} \leftrightarrows CO_2 + S_2O_8^{3\bullet-}$	1.8 x 10^{42}	1 x 10^5 $M^{-1}s^{-1}$ (34)
12	$C_2O_4^{\bullet-} \leftrightarrows CO_2 + CO_2^{\bullet-}$	1.2 x10^{12}	5.5 x 10^5 s^{-1} (22)
24	$Ru(NH_3)_6^{3+} + CO_2^{\bullet-} \rightleftarrows Ru(NH_3)_6^{2+} + CO_2$	2.2 x 10^{33}	> 1 x 10^7 $M^{-1}s^{-1}$

[a] See Supporting Information, Section 11 for references and details regarding the calculation of K_{eq} values.

[b] Literature sources for k_f values indicated by reference numbers in parentheses. The value of k_f for reaction 24 was obtained from the optimal fit of FD simulations to CV data, e.g., Figure 8.

FD simulations of the CV response require input of the diffusivities (D) of the various species. D for $C_2O_4^{2-}$ in an aqueous 0.1 M K_2SO_4 solution was reported by Compton and co-workers to be 1.03 x 10^{-5} cm^2/s. [21] The same value was assumed for $C_2O_4^{\bullet-}$. The diffusivity of CO_2 has been measured from CO_2 reduction at a Hg electrode in a DMF solution by Savéant and coworkers and reported to be 2.2 x 10^{-5} cm^2/s.[35] This value was adjusted to 2.5 x 10^{-6} cm^2/s using the Stokes-Einstein equation and the dynamic viscosities (η) of H_2O and DMF (see Supporting Information for additional details), and was further assumed for the diffusivity for $CO_2^{\bullet-}$. Values of D for $S_2O_8^{2-}$, $S_2O_8^{3\bullet-}$, SO_4^{2-}, and $SO_4^{\bullet-}$ in 0.1 M Na_2SO_4 were all assumed to be 1x10^{-5} cm^2/s based on the range of D values reported for $S_2O_8^{2-}$ in aqueous solutions (~0.6–1.4x10^{-5} cm^2/s).[17] An E^0 of –0.197 V vs Ag/AgCl for the $Ru(NH_3)_6^{3+/2+}$ redox couple and diffusion coefficients of

5.7 x 10^{-6} and 8.8 x 10^{-6} cm^2/s, respectively, for $Ru(NH_3)_6^{3+}$ and $Ru(NH_3)_6^{2+}$ were used.[26, 36] The heterogeneous reduction of $Ru(NH_3)_6^{3+}$, eq 17, is fast and kinetically reversible at the moderately low scan rates used in this study, Figure 1. We found that the FD simulations were insensitive to any value of the heterogeneous rate constant, k^0, above 1 cm/s. A value of 17 cm/s was used throughout to ensure that $Ru(NH_3)_6^{3+}$ occurs at the diffusion-limit rate under all simulation conditions. All FD simulations were performed using the commercial software, Digisim® (Version 3.0.3b, Bioanalytical Systems, Inc.). Additional details of simulations parameters are found in the Supporting Information.

Prior to simulating the entire autocatalytic reaction (eqs 17, 18, 19, 8, 15, 12, 24, and 16, shown in Scheme 4), we initially simulated the reversible CV response of $Ru(NH_3)_6^{3+}$ reduction, eq 17, at 50, 100, and 250 mV/s, in the absence of $S_2O_8^{2-}$ and $C_2O_4^{2-}$, obtaining excellent agreement between simulation and experiment (Figure S15). Then, eqs 18, 8, 9, and 19 were added to the simulation to capture the voltammetric behavior for the catalytic reduction of $S_2O_8^{2-}$ by $Ru(NH_3)_6^{2+}$ in the absence of $C_2O_4^{2-}$. The blue and dashed curves in Figure 8A shows an example of the experimental and simulated CVs, again demonstrating excellent agreement (additional comparisons of experimental and simulated CVs obtained for the same conditions at scan rates between 50 and 250 mV/s are presented in Figure S16).

The CV response for the entire autocatalytic reaction, Scheme 4, was simulated by inclusion of eqs 15, 12, 24, and 16, with the only unknown rate constant being that for reaction 24 ($Ru(NH_3)_6^{3+} + CO_2^{\bullet -} \rightleftarrows Ru(NH_3)_6^{2+} + CO_2$). By varying the value of the rate constant for eq 24, we found that using a value of k_f^{24} greater than 1 x 10^7 $M^{-1}s^{-1}$ yielded the best fit to the experimental voltammograms, as shown in Figure S17. As clearly evident by inspection of Figure 8, the 8-step mechanism shown in Scheme 4, with the rate constants listed in Table 1 precisely captures the CV

behavior of solutions containing 0.54 mM $Ru(NH_3)_6^{2+}$, 1.0 mM $S_2O_8^{2-}$, and 0 to 220 mM $C_2O_4^{2-}$. Simulations carried out under the same solution conditions at scan rates of 50 and 250 mV/s also provide excellent agreement between experiment and simulation, Figure S18.

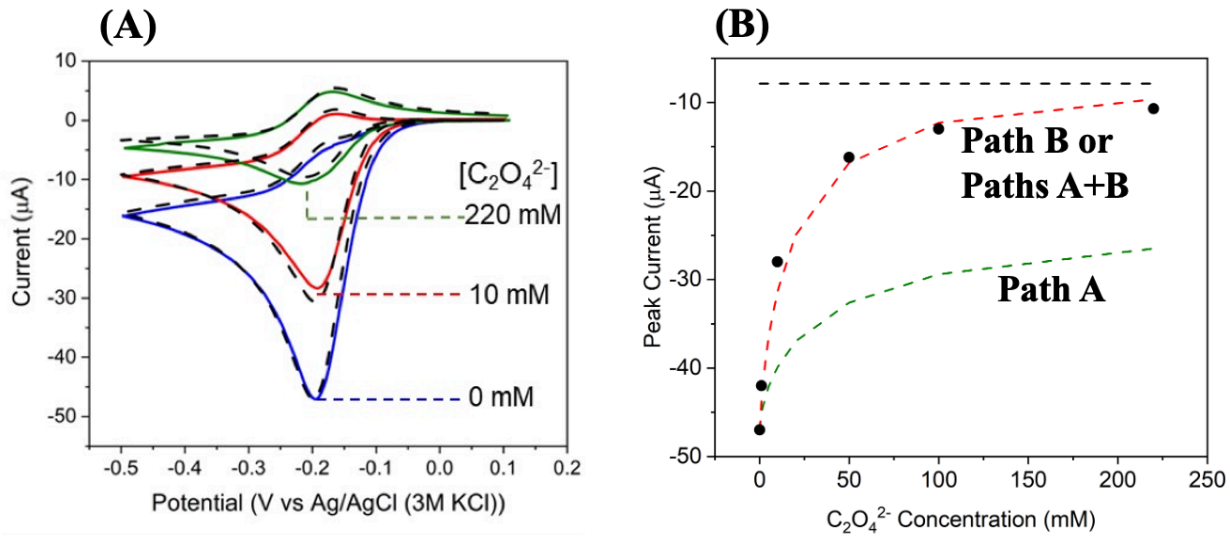

Figure 8. (A) Cyclic voltammetry of a solution containing 0.54 mM $Ru(NH_3)_6^{3+}$, 1.0 mM $S_2O_8^{2-}$, and 0.0 (blue solid line), 10 (red solid line), and 220 mM $C_2O_4^{2-}$ (green solid line). Simulated voltammograms are represented by black dashed lines. (B) Plot of i_{pc} vs. $[C_2O_4^{2-}]$. Black dots represent the experimental values of i_{pc} for CVs recorded with 0.0, 1.0, 10, 50, 100, and 220 mM $C_2O_4^{2-}$ in the presence of 0.54 mM $Ru(NH_3)_6^{3+}$ and 1.0 mM $S_2O_8^{2-}$. Simulated values of i_{pc} shown as the red dashed line, were performed using either eqs 17, 18, 8, 15, 12, 19, and 16 (Path A, green dashed line in Scheme 4), eqs 17, 18, 8, 15, 12, 19, and 24 (Path B, red dashed lines in Scheme 4), or eqs 17, 18, 8, 15, 12, 19, 24, and 16 (both Path A and Path B). Note that the simulation peak current values for Path B and a combination of Paths A and B are identical. Details of the digital simulation parameters are provided in Table 1. The full CV simulations in part (A) are obtained assuming Path B or a combination of Paths A and B. All voltammograms were recorded at 100 mV/s in an O_2-free aqueous solution containing 0.1 M Na_2SO_4 (pH = 6.8) with a 1.49 mm-radius GC working electrode.

To determine if either path A or path B in Scheme 4 is dominant in the autocatalytic cycle, the goodness of fit of the digital simulations to experimental CVs was examined as a function of the initial steps of paths A and B, k_f^{16} and k_f^{24}, respectively. Figure 8B shows a comparison of the

experimental voltammetric peak currents in solutions containing 0.54 mM $Ru(NH_3)_6^{2+}$, 1.0 mM $S_2O_8^{2-}$, and six different concentrations of $C_2O_4^{2-}$, ranging from 0 to 220 mM $C_2O_4^{2-}$, to the FD simulations with either path A or Path B removed from the mechanism (Scheme 1). To simulate path B alone, the rate of the direct reduction of $S_2O_8^{2-}$ by $CO_2^{\bullet-}$ in path A was set to zero, *i.e.*, $k_f^{16} = 0\ M^{-1}s^{-1}$. We found that eliminating path A had no effect the simulated peak currents (red dashed line). Conversely, eliminating path B by setting the rate constant for the reduction of $Ru(NH_3)_6^{3+}$ by $CO_2^{\bullet-}$ to zero, *i.e.*, $k_f^{24} = 0\ M^{-1}s^{-1}$, resulted in an ~50% decrease in the simulated currents. These results suggest that that $Ru(NH_3)_6^{3+/2+}$-mediated reduction of $S_2O_8^{2-}$ by $CO_2^{\bullet-}$, path B (eq 24 followed by eq 18) is the dominant path in the autocatalytic mechanism. This finding, based on analysis of the CV data, is consistent with the rate constant for the reduction of $Ru(NH_3)_6^{3+}$ by $CO_2^{\bullet-}$ (*i.e.*, the first step of path B, $k_f^{24} > 10^7\ M^{-1}s^{-1}$, Table 1), being at least two orders of magnitude larger than the rate constant for the reduction of $S_2O_8^{2-}$ by $CO_2^{\bullet-}$, k_f^{16} ($1 \times 10^5\ M^{-1}s^{-1}$). While DFT calculations indicate that the second step of path B (*i.e.*, eq. 18, $Ru(NH_3)_6^{2+} + S_2O_8^{2-} \rightleftarrows Ru(NH_3)_6^{3+} + S_2O_8^{3\bullet-}$) has a larger activation energy (62 kJ/mol) than that for the reduction of $S_2O_8^{2-}$ by $CO_2^{\bullet-}$ (43 kJ/mol), the fact that eq 24 is essentially irreversible ($K_{eq} = 2.2 \times 10^{33}$, Table 1) and more facile than eq 16, forces the autocatalytic reaction to proceed through path B. As noted above, we find that the simulated voltammograms using just path B (shutting off path A) are identical to those computed using both A and B. Thus, we conclude that the direct reduction of $S_2O_8^{2-}$ by $CO_2^{\bullet-}$, eq 16, does not significantly contribute to the overall $S_2O_8^{2-}/C_2O_4^{2-}$autocatalytic reaction on the time scale and conditions of the voltametric experiments reported herein.

We also considered the possible role of the direct reduction of $SO_4^{\bullet-}$ (eq 9) and direct oxidation of $CO_2^{\bullet-}$ (eq 13) at the GC electrode, in addition to the dimerization of $CO_2^{\bullet-}$ (eq 25), and electron transfer between $CO_2^{\bullet-}$ and $SO_4^{\bullet-}$ (eq 26). FD simulations of the concentration profiles

$CO_2^{\bullet-}$ and $SO_4^{\bullet-}$ at –0.35 V vs Ag/AgCl demonstrate that both $CO_2^{\bullet-}$ and $SO_4^{\bullet-}$ exist at ~1 nM (or lower) concentrations during the voltammetric scan, as shown in Figures 9A, B, and C and S22. Consequently, the flux of both species to the electrode is negligible (*i.e.*, the current generated by eqs 9 and 13 is too small to be measured). The reaction rate for eqs 25 and 26 can be estimated as $R^{24} = k_f^{24}[SO_4^{\bullet-}][CO_2^{\bullet-}]$ and $R^{25} = k_f^{25}[CO_2^{\bullet-}]^2$, respectively. Assuming diffusion-controlled reactions with $k_f^{24} \sim k_f^{25} \sim 10^{10}$ $M^{-1}s^{-1}$, along with $[CO_2^{\bullet-}] \sim [SO_4^{\bullet-}] \sim 10^{-9}$ M, yields $R^{24} = R^{25} \sim 10^{-8}$ M/s, indicating that eqs 24 and 25 do not occur to any appreciable extent. Figures S20 and S21 demonstrate that inclusion of these four "side reactions" have no impact on the fit of the FD simulations to the experimental CVs, as expected.

$$2\ CO_2^{\bullet-} \rightarrow C_2O_4^{2-} \qquad (25)$$

$$CO_2^{\bullet-} + SO_4^{\bullet-} \rightarrow CO_2 + SO_4^{2-} \qquad (26)$$

Concentration profiles for all reaction species involved in the autocatalytic reaction were computed from digital simulations and are displayed in Figure 9 and S22. In a solution containing 0.54 mM $Ru(NH_3)_6^{3+}$, 1.0 mM $S_2O_8^{2-}$, and 1.0 mM $C_2O_4^{2-}$, Figure 9A shows that the concentration of $Ru(NH_3)_6^{2+}$ decays from 0.54 mM to 0 mM within 15 µm from the working electrode (compared to a distance of ~100 µm in the absence of $S_2O_8^{2-}$, as seen in Figure S15B), indicating that electrogenerated $Ru(NH_3)_6^{2+}$ efficiently reduces $S_2O_8^{2-}$ under these solution conditions. Additionally, Figure 9A shows that the concentration of $C_2O_4^{2-}$ decreases relative to its bulk value ~50 µm from the electrode surface, consistent with consumption of $C_2O_4^{2-}$ via the autocatalytic reaction.

The concentration profiles of the $SO_4^{\bullet-}$ (Figure 9B) and the $CO_2^{\bullet-}$ (Figure 9C) were examined at different concentrations of $C_2O_4^{2-}$, again in the presence of 0.54 mM $Ru(NH_3)_6^{3+}$ and 1.0 mM $S_2O_8^{2-}$. In the absence of $C_2O_4^{2-}$, the concentration of $SO_4^{\bullet-}$ reaches a maximum value of 7.4 nM at a distance of 52 μm from the electrode surface (Figure 9B, black trace). Then, the maximum concentration of $SO_4^{\bullet-}$ decreases to 2.4 nM in the presence of 1 mM $C_2O_4^{2-}$ (Figure 9B, blue trace) and to 0.08 nM in the presence of 220 mM $C_2O_4^{2-}$ (Figure 9B, red trace and inset). Overall, as the concentration of $C_2O_4^{2-}$ increases, the concentration of $SO_4^{\bullet-}$ present in solution shows a marked decrease, demonstrating that $SO_4^{\bullet-}$ is reacting with $C_2O_4^{2-}$ via eqs 24 and 18. Figure 9C demonstrates that increasing the concentration of $C_2O_4^{2-}$ from 1.0 mM to 220 mM results in sub-nM concentrations of $CO_2^{\bullet-}$ in solution (0.01 nM at 1.0 mM $C_2O_4^{2-}$ to 0.1 nM at 220 mM $C_2O_4^{2-}$). This finding is again consistent with the proposed $S_2O_8^{2-}/C_2O_4^{2-}$ autocatalytic reaction mechanism where $C_2O_4^{2-}$ is oxidized by $SO_4^{\bullet-}$ (eq 15), resulting in the generation of $CO_2^{\bullet-}$ in solution (eq 12).

The concentration profiles of $Ru(NH_3)_6^{3+}$ and $Ru(NH_3)_6^{2+}$ as a function of the initial concentration of $C_2O_4^{2-}$ (with the concentration of $S_2O_8^{2-}$ held constant) were examined to understand why the CV response of a solution containing 0.54 mM $Ru(NH_3)_6^{3+}$, 1.0 mM $S_2O_8^{2-}$, and 220 mM $C_2O_4^{2-}$ closely resembles that of $Ru(NH_3)_6^{3+}$ alone, see Figure 2. In the absence of $S_2O_8^{2-}$ and $C_2O_4^{2-}$, the distance from the working electrode where equimolar concentrations of $Ru(NH_3)_6^{3+}$ and $Ru(NH_3)_6^{2+}$ are present is equal to ~28 μm, as shown by the dotted lines in Figure 9D. Then, in the presence of 1.0 mM $S_2O_8^{2-}$ and 1.0 mM $C_2O_4^{2-}$, the point of equimolar $Ru(NH_3)_6^{3+}$ and $Ru(NH_3)_6^{2+}$ shifts toward the working electrode to a distance of ~6 μm (Figure 9D, dashed lines). Upon increasing the $C_2O_4^{2-}$ concentration in solution to 220 mM, the concentration profiles of $Ru(NH_3)_6^{3+}$ and $Ru(NH_3)_6^{2+}$ (Figure 9D, solid line) nearly revert back to the profiles obtained

in the absence of $S_2O_8^{2-}$ and $C_2O_4^{2-}$. We conclude that in solutions containing $S_2O_8^{2-}$ and a large excess of $C_2O_4^{2-}$, the self-sustaining $S_2O_8^{2-}/C_2O_4^{2-}$ autocatalytic reaction cycle is effectively decoupled from the electrode redox reaction (reduction of $Ru(NH_3)_6^{3+}$) leading to a voltammetric response that is nearly indistinguishable from that of a solution containing only $Ru(NH_3)_6^{3+}$. It is worth noting that this observation is consistent with the electrolysis results obtained in Figure 6, which show that, within the detection limit of the experiment, no $S_2O_8^{2-}$ is directly reduced at the electrode when 220 mM $C_2O_4^{2-}$ is present in solution. Figure S22 presents additional concentration profile data, including expanded plots for $S_2O_8^{3\bullet-}$ and $C_2O_4^{\bullet-}$.

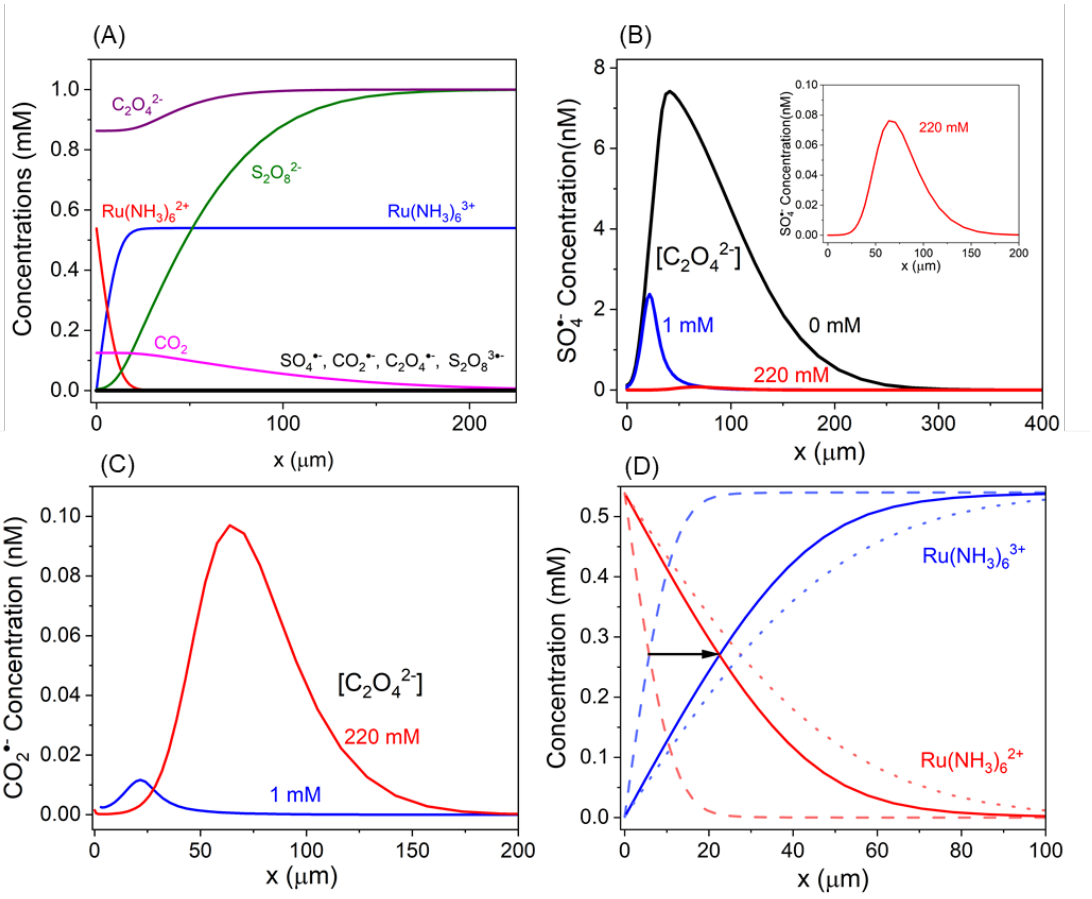

Figure 9. (A) Concentration profiles for a solution containing 0.54 mM $Ru(NH_3)_6^{3+}$, 1.0 mM $S_2O_8^{2-}$, and 1.0 mM $C_2O_4^{2-}$. Concentration profile of $C_2O_4^{2-}$ is shown in the purple, $S_2O_8^{2-}$ in green, $Ru(NH_3)_6^{3+}$ in blue, $Ru(NH_3)_6^{2+}$ in red, and CO_2 in pink. The following species exist at low concentrations and are not visible (black line): $CO_2^{\bullet-}$, $SO_4^{\bullet-}$, $C_2O_4^{\bullet-}$, $S_2O_8^{3\bullet-}$ on the concentration scale used in part (A). (B) Concentration profiles of $SO_4^{\bullet-}$, plotted on an expanded concentration scale, for solutions containing 1.0 mM $S_2O_8^{2-}$, 0.54 mM $Ru(NH_3)_6^{3+}$ with 0.0 mM $C_2O_4^{2-}$ (black line), 1.0 mM $C_2O_4^{2-}$ (blue line), and 220 mM $C_2O_4^{2-}$ (red line). (C) $CO_2^{\bullet-}$concentration profiles, plotted on an expanded concentration scale, for solutions containing 1.0 mM $S_2O_8^{2-}$, 0.54 mM $Ru(NH_3)_6^{3+}$ and either 1 mM $C_2O_4^{2-}$ (blue line) and 220 mM $C_2O_4^{2-}$ (red line). (D) Concentration profiles of $Ru(NH_3)_6^{3+}$ (blue lines) and $Ru(NH_3)_6^{2+}$ (red lines), in solutions containing 0.54 mM $Ru(NH_3)_6^{3+}$ in the absence (dotted lines) and presence of either 1.0 mM $S_2O_8^{2-}$ and 1.0 mM $C_2O_4^{2-}$ (dashed lines) or 1.0 mM $S_2O_8^{2-}$ with 220 mM $C_2O_4^{2-}$ (solid lines). Simulated concentration profiles were obtained at –0.35 V vs Ag/AgCl (3 M KCl), at a scan rate of 100 mV/s, and with 1.49 mm-radius working electrode. Further details of digital simulation parameters and conditions are shown in Supporting Information Table S5.

Lastly, we note that the finite-difference simulations of the concentration profiles of reactants ($S_2O_8^{2-}$ and $C_2O_4^{2-}$) and products (SO_4^{2-} and CO_2) as a function of time strongly indicates that the $S_2O_8^{2-}/C_2O_4^{2-}$ autocatalytic reaction shown in Scheme 4 results in a chemical traveling wave that, once initiated, propagates away from the electrode at a nearly constant velocity. For example, Figure 10 shows simulated CV concentration profiles for $S_2O_8^{2-}$ (black curves) and SO_4^{2-} (blue curves) for a solution containing 0.54 mM $Ru(NH_3)_6^{3+}$, 1.0 mM $S_2O_8^{2-}$, and 220 mM $C_2O_4^{2-}$ at a scan rate of 100 mV/s. As before, the CV was started at E = 0.10 V vs Ag/AgCl and was scanned at 100 mV/s in the negative reduction to reduce $Ru(NH_3)_6^{3+}$. The solid lines represent concentration profiles obtained at the switching potential (–0.50 V), while the dashed lines correspond to the concentration profiles ~6 s later at the end of the CV, when the electrode potential had returned to 0.10 V. The dashed lines clearly show that $S_2O_8^{2-}$ is fully consumed at distances up to 150 μm from the electrode surface at the end of the CV. The simulations were continued for an additional 6 seconds, resulting in $S_2O_8^{2-}$ and SO_4^{2-} profiles that have essentially

the same shape as at the end of the CV, but now shifted an additional ~100 μm from the surface. Since no electrons are being injected into the solution (via $Ru(NH_3)_6^{3+}$ reduction) during this latter 6 second period, it is clear that the translocation of the concentration profiles is due to a self-sustaining reaction. From the shift in the concentration profiles between t = 6 and 12 s, we estimate that the traveling wave velocity is ~18 μm/s. Self-propagating chemical waves are known to be associated with autocatalytic chemical systems, with the chemical wave velocity determined by the kinetics of the autocatalytic reaction.[37-40]

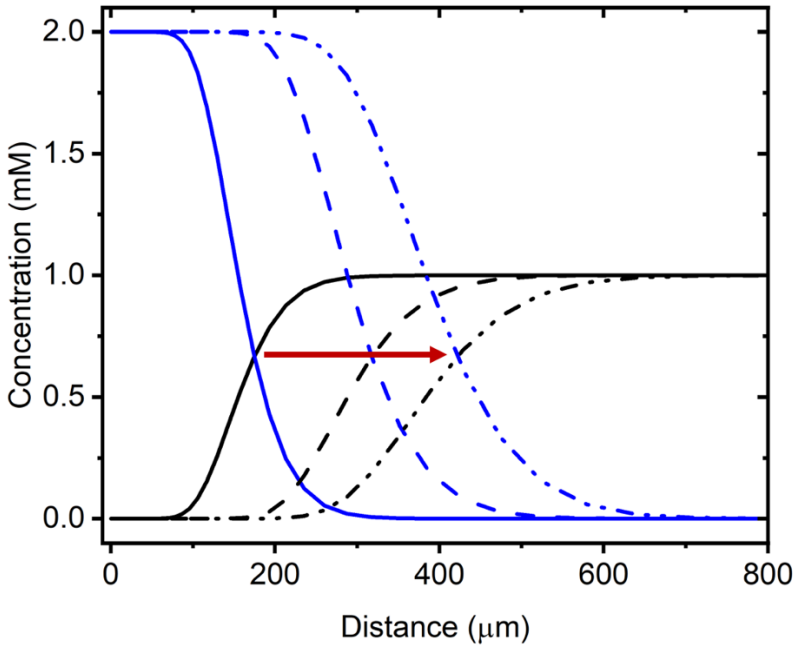

Figure 10. Simulated concentration profiles for $S_2O_8^{2-}$ (black curves) and SO_4^{2-} (blue curves) for a solution containing 0.54 mM $Ru(NH_3)_6^{3+}$, 1.0 mM $S_2O_8^{2-}$, and 220 mM $C_2O_4^{2-}$ at a scan rate of 100 mV/s. The solid lines represent concentration profiles obtained at the switching potential (–0.50 V), the dashed lines are the concentration profiles ~6 s later at the end of the CV (0.10 V), and the dashed-dotted lines are the concentration profiles another ~6 s later, for a total of t = 12 s after the switching potential, at 0.70 V. The red arrow indicates that the concentration profiles of $S_2O_8^{2-}$ and SO_4^{2-} are traveling through solution as the voltammogram proceeds.

Conclusions

We have demonstrated the $S_2O_8^{2-}/C_2O_4^{2-}$ autocatalytic reaction can be effectively initiated by the mediated one-electron reduction of $S_2O_8^{2-}$ using the $Ru(NH_3)_6^{3+/2+}$ redox couple. DEMS analysis unambiguously demonstrates that the $S_2O_8^{2-}/C_2O_4^{2-}$ autocatalytic reaction is self-sustaining once initiated, generating CO_2 for up to 10 min. past initiation. Collection of CO_2 in the form of $BaCO_3$ during CPE experiments additionally demonstrates that the mediated reduction of $S_2O_8^{2-}$ in the presence of $C_2O_4^{2-}$ results in the generation of CO_2. Coulometric analysis of CPE experiments under optimized solution conditions suggests that the autocatalytic reaction is self-sustaining and can be initiated by a very small (unmeasurable within error) number of electrons injected into the solution.

A detailed mechanistic analysis was performed using DFT and AIMD simulations, which further guided FD simulations of experimental CV data. Based on activation energy barriers computed from DFT, we conclude that the reduction of $S_2O_8^{2-}$ by $CO_2^{\bullet-}$, which is accompanied by a high inner-sphere reorganization energy, must be slower than the oxidation of $C_2O_4^{2-}$ by $SO_4^{\bullet-}$, a conclusion supported by prior pulse radiolysis studies. In agreement with this conclusion, FD simulations of the experimental CVs show that the $S_2O_8^{2-}/C_2O_4^{2-}$ autocatalytic reaction proceeds via the reduction of $Ru(NH_3)_6^{3+}$ by $CO_2^{\bullet-}$ followed by the reduction of $S_2O_8^{2-}$ by $Ru(NH_3)_6^{2+}$ (eq 24 followed by eq 18) rather than by the reduction of $S_2O_8^{2-}$ by $CO_2^{\bullet-}$ (eq 16).

FD simulated concentration profiles suggest that the autocatalytic reaction generates a chemical traveling wave consisting of the reactants ($S_2O_8^{2-}$ and $C_2O_4^{2-}$) and products (SO_4^{2-} and CO_2) under appropriate solution conditions. Experimental demonstration and detailed analyses of the traveling wave associated with the $S_2O_8^{2-}/C_2O_4^{2-}$ autocatalytic reaction is underway and will be reported elsewhere.

Associated Content

Data Availability Statement

The first-principles data generated in this study has been made publicly available on the ioChem server (https://doi.org/10.19061/ iochem-bd-6-144) and includes input and output files. The python codes for analyzing molecular dynamics simulations are available at https://github.umn.edu/tanwa008/analyzing_aimd_simulations-. Additionally, all data for product characterization and parameters for model and computational efforts can be found in the Supporting Information.

Supporting Information

The Supporting Information is available free of charge at (insert link to paper).

Details of CV studies, calculation of thermodynamic and kinetic parameters, differential electrochemical mass spectrometry studies, procedure used for CPE and CO_2 detection, DFT calculations, and parameters used for digital simulation of cyclic voltammograms (PDF link to SI).

Author Information

Corresponding Authors

Héctor D. Abruña − *Department of Chemistry and Chemical Biology, Cornell University, Ithaca, New York 14850, United States;* https://orcid.org/0000-0002-3948-356X; Email: hda1@cornell.edu

Matthew Neurock − *Department of Chemical Engineering and Materials Science and Department of Chemistry, University of Minnesota, Minneapolis, Minnesota 55455, United States;* https://orcid.org/0000-0003-1458-7837; Email: mneurock@umn.edu

Henry S. White − *Department of Chemistry, University of Utah, Salt Lake City, Utah 84112, United States;* https://orcid.org/0000-0002-5053-0996; Email: white@chemistry.utah.edu

Authors

Jordyn N. Janusz – *Department of Chemistry, University of Utah, Salt Lake City, Utah 84112, United States;* https://orcid.org/0000-0001-7788-4754

Joshua A. Beeler – *Department of Chemistry, University of Utah, Salt Lake City, Utah 84112, United States;* https://orcid.org/0009-0001-9882-3173

Seyyedamirhossein Hosseini – *Department of Chemistry, University of Utah, Salt Lake City, Utah 84112, United States*; https://orcid.org/0000-0002-3617-2547

Mayank Tanwar – *Department of Chemical Engineering and Materials Science and Department of Chemistry, University of Minnesota, Minneapolis, Minnesota 55455, United States;* https://orcid.org/0000-0003-2205-6016

Rui Zeng – *Department of Chemistry and Chemical Biology, Cornell University, Ithaca, New York 14850, United States;* https://orcid.org/0000-0002-7577-767X

Hongsen Wang – *Department of Chemistry and Chemical Biology, Cornell University, Ithaca, New York 14850, United States;* https://orcid.org/0000-0001-7926-2895

Complete contact information is available at: (link to paper).

Author Contributions

∇ J.N.J. and J.A.B. contributed equally to this work.

Notes: The authors declare no competing financial interest.

Acknowledgements

This work was supported by the National Science Foundation Center for Synthetic Organic Electrochemistry (CHE-2002158). M. T. acknowledges the Doctoral Dissertation Fellowship from the University of Minnesota. M. T. and M. N. acknowledge the Minnesota Supercomputing Institute (MSI) at the University of Minnesota for the computational resources.

References

(1) Kempf, R. Oxydationen mit Silberperoxyd. I. Die Oxydation von Oxalsäure. *Berichte der deutschen chemischen Gesellschaft* **1905**, *38* (4), 3963–3966.
(2) King, C. V. SILVER ION CATALYSIS OF PERSULFATE OXIDATIONS. IV. OXIDATION OF OXALATE ION1. *J. Am. Chem. Soc.* **1928**, *50* (8), 2089–2099.
(3) Allen, T. L. The oxidation of oxalate ion by peroxydisulfate1. *J. Am. Chem. Soc.* **1951**, *73* (8), 3589–3593.
(4) Yost, D. M. CATALYSIS BY SILVER ION OF THE OXIDATION OF CHROMIC SALTS BY PEROXYSULFURIC ACID. THE EXISTENCE OF TRIVALENT SILVER COMPOUNDS. *J. Am. Chem. Soc.* **1926**, *48* (1), 152–164.
(5) Yost, D. M. The Catalytic Effect of Silver Ammonia Ion in the Oxidation of Ammonia by Peroxysulfates. *J. Am. Chem. Soc.* **1926**, *48* (2), 374–383.
(6) Yost, D. M.; Claussen, W. H. Reduction of peroxysulfate by vanadyl ion with silver ion as catalyst. *J. Am. Chem. Soc.* **1931**, *53* (9), 3349–3354.
(7) Dekker, A. O.; Lévy, H. A.; Yost, D. M. Reduction of Peroxysulfate by Manganous Ion and by Hydrazine with Silver Ion as Catalyst. *J. Am. Chem. Soc.* **1937**, *59* (11), 2129–2131.
(8) Cone, W. The Reduction of Peroxydisulfate by Cerous Ion, Catalyzed by Silver Nitrate. *J. Am. Chem. Soc.* **1945**, *67* (1), 78.
(9) King, C. V. SILVER ION CATALYSIS OF PERSULFATE OXIDATIONS. I SALT EFFECT ON THE VELOCITY OF OXIDATION OF AMMONIA. II. COMPARISON OF THE VELOCITY WITH VARIOUS REDUCING AGENTS. *J. Am. Chem. Soc.* **1927**, *49* (11), 2689–2699.
(10) Memming, R. Mechanism of the electrochemical reduction of persulfates and hydrogen peroxide. *J. Electrochem. Soc.* **1969**, *116* (6), 785–790.
(11) Armstrong, D. A.; Huie, R. E.; Koppenol, W. H.; Lymar, S. V.; Merényi, G.; Neta, P.; Ruscic, B.; Stanbury, D. M.; Steenken, S.; Wardman, P. Standard electrode potentials involving radicals in aqueous solution: inorganic radicals (IUPAC Technical Report). *Pure and Applied Chemistry* **2015**, *87* (11-12), 1139–1150.
(12) Kanoufi, F.; Bard, A. J. Electrogenerated chemiluminescence. 65. An investigation of the oxidation of oxalate by tris (polypyridine) ruthenium complexes and the effect of the electrochemical steps on the emission intensity. *J. Phys. Chem. B* **1999**, *103* (47), 10469–10480.
(13) Chang, M.-M.; Saji, T.; Bard, A. J. Electrogenerated chemiluminescence. 30. Electrochemical oxidation of oxalate ion in the presence of luminescers in acetonitrile solutions. *J. Am. Chem. Soc.* **1977**, *99* (16), 5399–5403.
(14) Kolthoff, I.; Miller, I. The chemistry of persulfate. I. The kinetics and mechanism of the decomposition of the persulfate ion in aqueous medium1. *J. Am. Chem. Soc.* **1951**, *73* (7), 3055–3059.
(15) Herrera-Ordonez, J. The role of sulfate radicals and pH in the decomposition of persulfate in aqueous medium: A step towards prediction. *Chem. Eng. J. Adv.* **2022**, *11*, 100331.
(16) Crossey, L. J. Thermal degradation of aqueous oxalate species. *Geochim. Cosmochim. Acta* **1991**, *55* (6), 1515–1527.
(17) Shafiee, S. A.; Aarons, J.; Hamzah, H. H. Electroreduction of peroxodisulfate: A review of a complicated reaction. *J. Electrochem. Soc.* **2018**, *165* (13), H785–H798.
(18) Pendergast, A. D.; White, H. S. Double-Layer Inhibition of Peroxydisulfate Reduction at Mercury Ultramicroelectrodes. A Quantitative Analysis of the Frumkin Effect Including Molecular Transport and Long-Range Electron Transfer. *J. Phys. Chem. C* **2023**, *127*, 11283–11297.
(19) Hosseini, S.; Janusz, J. N.; Tanwar, M.; Pendergast, A. D.; Neurock, M.; White, H. S. Oxidation by reduction: efficient and selective oxidation of alcohols by the electrocatalytic reduction of peroxydisulfate. *J. Am. Chem. Soc.* **2022**, *144* (46), 21103–21115.
(20) Hosseini, S.; Beeler, J. A.; Sanford, M. S.; White, H. S. Electroorganic synthesis in aqueous solution *via* generation of strongly oxidizing and reducing intermediates. *Faraday Discuss.* **2023**, *247*, 195–208.
(21) Šljukić, B.; Baron, R.; Compton, R. G. Electrochemical determination of oxalate at pyrolytic graphite electrodes. *Electroanalysis* **2007**, *19* (9), 918–922.

(22) Kai, T.; Zhou, M.; Johnson, S.; Ahn, H. S.; Bard, A. J. Direct observation of $C_2O_4^{\bullet-}$ and $CO_2^{\bullet-}$ by oxidation of oxalate within nanogap of scanning electrochemical microscope. *J. Am. Chem. Soc.* **2018**, *140* (47), 16178–16183.
(23) Kanoufi, F.; Cannes, C.; Zu, Y.; Bard, A. J. Scanning Electrochemical Microscopy. 43. Investigation of Oxalate Oxidation and Electrogenerated Chemiluminescence across the Liquid− Liquid Interface. *J. Phys. Chem. B* **2001**, *105* (37), 8951–8962.
(24) Bocarsly, A. R. P. a. A. B. High-Efficiency Conversion of CO_2 to Oxalate in Water is Possible Using a Cr-Ga Oxide Electrocatalyst. *ACS Catal.* **2019**, *9*, 2324–2333.
(25) Feldberg, S. W.; Jeftic, L. Nuances of the ECE mechanism. IV. Theory of cyclic voltammetry and chronoamperometry and the electrochemical reduction of hexacyanochromate (III). *J. Phys. Chem.* **1972**, *76* (17), 2439–2446.
(26) Wang, Y.; Limon-Petersen, J. G.; Compton, R. G. Measurement of the diffusion coefficients of $[Ru(NH_3)_6]^{3+}$ and $[Ru\ (NH_3)_6]^{2+}$ in aqueous solution using microelectrode double potential step chronoamperometry. *J. Electroanal. Chem.* **2011**, *652* (1-2), 13–17.
(27) Hosseini, S.; Solymosi, G., T; White, H. S. Investigation of the Electrocatalytic Reduction of Peroxydisulfate Using Scanning Electrochemical Microscopy. *Anal. Chem.* **2024**.
(28) Zeng, R.; Yang, Y.; Shen, T.; Wang, H.; Xiong, Y.; Zhu, J.; Wang, D.; Abruña, H. D. Methanol Oxidation Using Ternary Ordered Intermetallic Electrocatalysis: A DEMS Study. *ACS Catal* **2020**, *10*, 770–776.
(29) Kresse, G.; Hafner, J. *Ab initio* molecular dynamics for liquid metals. *Phys. Rev. B* **1993**, *47*, 558.
(30) Gaussian 16, Revision A.03, M. J. Frisch, G. W. Trucks, H. B. Schlegel, G. E. Scuseria, M. A. Robb, J. R. Cheeseman, G. Scalmani, V. Barone, G. A. Petersson, H. Nakatsuji, X. Li, M. Caricato, A. V. Marenich, J. Bloino, B. G. Janesko, R. Gomperts, B. Mennucci, H. P. Hratchian, J. V. Ortiz, A. F. Izmaylov, J. L. Sonnenberg, D. Williams-Young, F. Ding, F. Lipparini, F. Egidi, J. Goings, B. Peng, A. Petrone, T. Henderson, D. Ranasinghe, V. G. Zakrzewski, J. Gao, N. Rega, G. Zheng, W. Liang, M. Hada, M. Ehara, K. Toyota, R. Fukuda, J. Hasegawa, M. Ishida, T. Nakajima, Y. Honda, O. Kitao, H. Nakai, T. Vreven, K. Throssell, J. A. Montgomery, Jr., J. E. Peralta, F. Ogliaro, M. J. Bearpark, J. J. Heyd, E. N. Brothers, K. N. Kudin, V. N. Staroverov, T. A. Keith, R. Kobayashi, J. Normand, K. Raghavachari, A. P. Rendell, J. C. Burant, S. S. Iyengar, J. Tomasi, M. Cossi, J. M. Millam, M. Klene, C. Adamo, R. Cammi, J. W. Ochterski, R. L. Martin, K. Morokuma, O. Farkas, J. B. Foresman, and D. J. Fox, Gaussian, Inc., Wallingford CT, 2016. (accessed 2021-06-01).
(31) Marcus, R. On the Theory of Oxidation-Reduction Reactions Involving Electron Transfer. *J. Chem. Phys.* **2004**, *24*, 996.
(32) Bard, A.; Faulkner, L.; White, H. *Electrochemical Methods: Fundamentals and Applications*; Wiley, 2022.
(33) Huie, R. E.; Clifton, C. L. Kinetics of the reaction of the sulfate radical with the oxalate anion. *International journal of chemical kinetics* **1996**, *28* (3), 195-199.
(34) Buxton, G. V.; Salmon, G. A.; Wood, N. D. A pulse radiolysis study of the chemistry of oxysulphur radicals in aqueous solution. *Physico-Chemical Behaviour of Atmospheric Pollutants: Air Pollution Research Reports* **1990**, 245-250.
(35) Gennaro, A.; Isse, A. A.; Severin, M.-G.; Vianello, E.; Bhugun, I.; Savéant, J.-M. Mechanism of the electrochemical reduction of carbon dioxide at inert electrodes in media of low proton availability. *Faraday Trans.* **1996**, *92* (20), 3963–3968.
(36) Sun, P.; Mirkin, M. V. Kinetics of electron-transfer reactions at nanoelectrodes. *Anal. Chem.* **2006**, *78* (18), 6526–6534.
(37) Billingham, J.; King, A. C. Chemical and Electrochemical Waves. In *Wave Motion*, Crighton, D. G. Ed.; Cambridge University Press, 2000; pp 308–352.
(38) Saul, A.; Showalter, K. Propagating Reaction-Diffusion Fronts. In *Oscillations and Traveling Waves in Chemical Systems*, Field, R. J. Ed.; John Wiley & Sons, Inc., 1985; pp 419–439.
(39) Agladze, K.; Thouvenel, S.; Steinbock, O. Electrochemical Waves on Patterned Surfaces: Propagation through Narrow Channels. *J. Phys. Chem. A* **2001**, *105*, 7356–7363.

(40) Kuze, M.; Horisaka, M.; Suematsu, N. J.; Amemita, T.; Steinbock, O.; Nakata, S. Chemical Wave Propagation in the Belousov–Zhabotinski Reaction Controlled by Electrical Potential. *J. Phys. Chem. A* **2018**, *123*, 4853–4857.